DESIGN OF A PASSIVE SELF-TUNING LEVER-TYPE VIBRATION ISOLATION SYSTEM

by

Ahmet Onur Özyar

B.S., Mechanical Engineering, Middle East Technical University, 2008

Submitted to the Institute for Graduate Studies in
Science and Engineering in partial fulfillment of
the requirements for the degree of
Master of Science

Graduate Program in Mechanical Engineering
Boğaziçi University

2019

DESIGN OF A PASSIVE SELF-TUNING LEVER-TYPE VIBRATION ISOLATION SYSTEM

APPROVED BY

Assoc. Prof. Çetin Yılmaz …….

(Thesis supervisor)

Assist. Prof. Evren Samur …….

Assist. Prof. Polat Şendur …….

DATE OF APPROVAL …….

ACKNOWLEDGEMENTS

I would like to gratefully thank my thesis supervisor Assoc. Prof. Çetin Yılmaz for his kindness, understanding and support. His guidance and patience were invaluable to me at all stages of this thesis.

I would like to thank the members of my thesis committee Assist. Prof. Evren Samur and Assist. Prof. Polat Şendur for their contributions. I am thankful to all my friends, colleagues, research assistants and the staff at the mechanical engineering department. I would like to acknowledge Doruk Akarçay, Eren Adalı and Mehmet Atalay for their preliminary work on the vibro-impact actuator and Selamet Çevik for his support on the manufacture and development of the experimental set-up.

I am grateful to all my colleagues, supervisors and teachers who have contributed to the development of my engineering and academical skills. I would like to thank my friends who supported me during my graduate studies. I particularly want to acknowledge my old friend and library staff Necati Ort for his support both morally and with the library material.

Finally, I thank my family for their love, support and encouragement. I especially thank my wife for her endless support and encouragement during all parts of my graduate study, from the beginning to the end.

ABSTRACT

DESIGN OF A PASSIVE SELF-TUNING LEVER-TYPE VIBRATION ISOLATION SYSTEM

In this study, a novel self-tuning passive lever-type vibration isolation system for base excitations is described. Due to inertial coupling within the vibration isolation system, an antiresonance frequency is generated, which depends on the amplification ratio of the lever. At this frequency, the instant center of zero velocity of the lever coincides with the payload hinge point. As a result, the payload experiences minimum amount of vibration. When the excitation frequency changes, the system changes the lever ratio so as to bring the antiresonance frequency to coincide with the excitation frequency to suppress the output vibration. The designed mechanical system does not require any electronic sensors or actuators. The self-tuning operation is enabled by a vibro-impact type actuator powered by the input vibration rendering the system self-powered. This actuator is placed below the payload hinge and moves the lever in the appropriate direction to bring the instant center of zero velocity to the payload hinge position. Hence, the system achieves the optimum lever ratio for minimum vibration output. The equations of motion of the system are derived and the location of the instant center is obtained analytically. Then, multi-body dynamic simulations are carried out to verify the self-tuning response of the system. An experimental set-up incorporating a variable ratio lever, a softly suspended ground mass and a vibro-impact type actuator, is designed. Experimental results validate that the system always goes to antiresonance condition in the working frequency range.

ÖZET

KENDİ KENDİNİ AYARLAYABİLEN PASİF KALDIRAÇ TİPİ BİR TİTREŞİM İZOLATÖRÜNÜN TASARIMI

Bu çalışmada, tabandan gelen titreşimler için kendi kendini ayarlayabilen kaldıraç tipi bir titreşim izolatörü tanımlanmıştır. Titreşim izolasyon sistemi içindeki ataletsel bağlantı nedeniyle, kaldıracın mekanik kazanç oranına bağlı olan bir antirezonans frekansı üretilir. Sisteme antirezonans frekansında tahrik uygulandığında, kaldıracın ani dönme merkezi, yük taşıma mafsalı ile çakışmaktadır. Sonuç olarak, taşınan yük minimum miktarda titreşim yaşar. Gelen tahrik frekansı değiştiğinde, sistem antirezonans frekansını, çıkış titreşimini bastırmak için tahrik frekansıyla çakışmaya getirmek için kaldıraç oranını değiştirir. Tasarlanan mekanik sistem elektronik sensör veya tahrik gerektirmemektedir. Kendi kendine ayar işlemi, girişteki titreşimi darbeye çeviren ve dışarıdan enerji gerektirmeden bir aktüatör tarafından sağlanmaktadır. Kullanılan aktüatör, yük taşıma mafsalının altında konumlandırılmakta ve üzerindeki kauçuk takozlar yardımı ile ani dönme merkezini bulunduğu konuma yaklaştıracak şekilde kaldıraç oranını değiştirmektedir. Çalışmada öncelikle sistemin hareket denklemleri çıkarılmış ve ani dönme merkezinin konumu analitik olarak elde edilmiştir. Ardından, ani dönme merkezinin yük taşıma mafsalına yaklaştırılmasına dayalı algoritmanın doğrulanması için dinamik simülasyonlar yapılmıştır. Deneysel doğrulama için esnek bağlantılı mafsallar yardımı ile değişken kaldıraç oranlı bir izolatör geliştirilmiştir. Yumuşak yaylar ile askıda bırakılmış bir kütle, atalet referans mekanizmasını canlandırarak hem sensör hem de aktüatör olarak işlev görmüştür. Deneysel sonuçlar, sistemin çalışma frekansı aralığında her zaman antirezonans durumuna gittiğini doğrulamaktadır.

TABLE OF CONTENTS

ACKNOWLEDGEMENTS iii

ABSTRACT iv

ÖZET v

TABLE OF CONTENTS vi

LIST OF FIGURES viii

LIST OF TABLES viii

LIST OF SYMBOLS xii

LIST OF ABBREVIATIONS xv

1. INTRODUCTION 1

    1.1. Objective and Motivation of Study 1

    1.2. Literature Review 2

    1.3. Overview of Thesis 10

2. THE DEVELOPMENT OF THE CONTROL ALGORITHM 11

    2.1. Lumped Model Equations for Type II Lever Type DAVI 11

    2.2. The Development of the Control Algorithm 14

3. NUMERICAL VERIFICATION 21

4. THE DESIGN OF EXPERIMENTAL SET-UP 27

    4.1. Distributed Parameter Model 27

    4.2. The Design of the Prototype System 30

        4.2.1. Sensor and Actuator Assembly 31

        4.2.2. The Payload Sub-Assembly 36

        4.2.3. The Base Sub-Assembly 43

        4.2.4. The Isolator Sub-Assembly 43

    4.3. Total System Response and the Critical Frequencies 44

5. EXPERIMENTAL RESULTS 46

6. CONCLUSION 53

6.1. Summary 53

6.2. Future Work 54

REFERENCES 56

LIST OF FIGURES

Figure 1.1. Type I (Left) and Type II (right) DAVI 4

Figure 2.1. Lumped parameter model of the lever-type isolator 11

Figure 2.2. The transmissibility and phase angle plot of a lever type vibration isolator with f_p=15 Hz, f_z=18.75 Hz, μ=0.1, α=5.82 where $\omega_p = 2\pi f_p$ and $\omega_z = 2\pi f_z$..... 14

Figure 2.3. Case1: Motion of the system for $\omega < \omega p < \omega z$. Here, $Y2 > Y1$..... 16

Figure 2.4. Case 2: Motion of the system for $\omega = \omega p < \omega z$. Here, $Y2 \to \infty$..... 16

Figure 2.5. Case 3: Motion of the system for $\omega p < \omega < \omega z$..... 16

Figure 2.6. Case 4: Motion of the system for $\omega p < \omega = \omega z$. Here, $Y2 = 0$ 17

Figure 2.7. Case 5: Motion of the system for $\omega p < \omega z < \omega$. Here, $Y1 > Y2$..... 17

Figure 2.8. Self-tuning operation of the lever (a) start, (b) progress (c) tuned system 19

Figure 2.9. Flowchart of the control algorithm 20

Figure 3.1. The representative system and locations of the dampers (marked with yellow curves) and forces (shown in red under the lever) 21

Figure 3.2. The selected frequencies (blue dashed lines) shown on the FRF plot of the system for amplitude 23

Figure 3.3. Time response for $\omega = 8$ Hz , i.e., $\omega < \omega p < \omega z$ 24

Figure 3.4. Time response for $\omega = 8.8$ Hz , i.e., $\omega = \omega p < \omega z$..... 24

Figure 3.5. Time response for $\omega = 11$ Hz , i.e., $\omega p < \omega < \omega z$ 24

Figure 3.6. Time response for $\omega = 11.9$ Hz , i.e., $\omega p < \omega = \omega z$ 25

Figure 3.7. Time response for $\omega = 20$ Hz , i.e., $\omega p < \omega z < \omega$ 25

Figure 4.1. The variables used in the prototype system. 27

Figure 4.2. The 3D model of the experimental set-up..... 30

Figure 4.3. The overall system and its sub-assemblies shown in different colors 31

Figure 4.4. The sensor and actuator assembly shown as the V-shaped part with rubber pads on the artificial ground mass. 32

Figure 4.5 The actuator forces created by impact and the wedge angle..... 32

Figure 4.6. Linear finite element analysis regarding the parallel motion of the inertia block assembly..... 35

Figure 4.7. The payload sub-assembly 36

Figure 4.8. The leaf springs (in blue) and their extensions (in red) forming rotation center..... 38

Figure 4.9. The exploded view of the hinge 38

Figure 4.10. The deformed geometry of hinges obtained by linear finite element analysis 39

Figure 4.11. Parameters for hinge calculations 40

Figure 4.12. The system frame and base 43

Figure 4.13. The lever in leftmost (100 mm position), middle (130mm) and rightmost (190mm) positions 44

Figure 5.1. The experimental set-up without the sensor and data logger 46

Figure 5.2. FRF for three different lever positions 47

Figure 5.3. Self-tuning of the system to 20 Hz input excitation 49

Figure 5.4. Self-tuning of the system to 30 Hz excitation 49

Figure 5.5. Response of the system during a frequency sweep from 30 Hz to 20 Hz at 10 Hz/min 50

Figure 5.6. Response of the system during a frequency sweep from 20 Hz to 30 Hz at 10 Hz/min 51

Figure 5.7. FRF of frequency sweep from 30 Hz to 20Hz 51

Figure 5.8. FRF of frequency sweep from 20 Hz to 30 Hz 52

Figure 5.9. Long exposure photograph of the set-up under constant frequency excitation 52

LIST OF TABLES

Table 4.1. Artificial ground system parameters 36

Table 4.2. Parameters and natural frequency calculations for payload..... 37

Table 4.3. The hinge parameters and stiffness calculations..... 42

Table 4.4. Gravitational center and mass moment of inertia calculations for the isolator..... 44

Table 4.5. Pole and zero frequencies for three different lever positions..... 44

Table 5.1. Pole and zero frequencies for three different lever positions..... 47

LIST OF SYMBOLS

a_1	length of the first link in 4-bar mechanism
a_2	length of the second link in 4-bar mechanism
a_3	length of the third link in 4-bar mechanism
d_1	length of the base (fourth link) in 4-bar mechanism
E	Young's modulus
F_1	control force pulling the lever to the left-hand side
F_2	control force pulling the lever to the right-hand side
F_{friction}	friction force defined on the lever
F_{n}	normal force in the wedge type impact actuator
F_{t}	tangential force in the wedge type impact actuator
G	location of the isolator's center of gravity
h	height of cantilever cross section
I_z	the rotational inertia of the lever
I_{xx}	second moment of inertia of cantilever cross section
k	total isolator stiffness
$k_{\text{cantilever}}$	stiffness of cantilever spring
k_{link}	the equivalent stiffness of a cantilever with moment and force loading at its tip
$k_{\theta,eq}$	total torsional stiffness of the hinge assembly
k_{eq}	total stiffness of the hinge assembly
L	length of cantilever spring
l_1	length of the lever further from the mass hinge
l_2	hinge spacing on the lever

l_3	distance between the base hinge and the isolator center of mass
l_{tot}	total length of the lever
l_{is}	location of isolator mass from the left end
M	payload mass
m_{ground}	the mass of the softly suspended block
m_{is}	the magnitude of the point mass at the tip of the lever
m_l	the mass of the lever
m_{payload}	the mass of the payload
t	time
T	kinetic energy
$Tr(\omega)$	transmissibility
u	the dead length of the lever beyond the base hinge
V	potential energy
w	width of the cantilever cross section
y_1	displacement of the base, excitation amplitude
y_2	displacement of the payload
y_3	displacement of the isolator's center of mass
Y_1	the amplitude of the excitation
Y_2	the amplitude of payload motion
α	the ratio of effective lever length to the length between hinges
β	the lever ratio
θ	angular displacement of the lever
θ_1	the angle of the first link in 4-bar mechanism
θ_2	the angle of the second link in 4-bar mechanism

θ_3	the angle of the third link in 4-bar mechanism
μ	the ratio of the isolator mass to the mass of the payload
$\mu_{friction}$	the friction coefficient in impact type actuator
φ	the wedge angle of the impact type actuator
$\emptyset$	phase angle
ω	excitation frequency
ω_0	the natural frequency of a mass-spring system with mass *M* and stiffness *k*
ω_p	resonance frequency (pole) of a system having a single pole
ω_z	anti-resonance frequency (zero) of a system having a single zero

LIST OF ACRONYMS / ABBREVIATIONS

AMD	auxiliary mass damper
AMS	auxiliary mass systems
ATVA	adaptive tuned vibration absorbers
CVT	continuously variable transmission
DAVI	dynamic anti-resonant vibration isolator
DOF	degree of freedom
DVA	dynamic vibration absorber
FRF	frequency response function
Hz	Hertz
LHS	left hand side
MBD	multi-body dynamics
RHS	right hand side
SDOF	single degree of freedom
MRE	magnetorheological elastomer

1. INTRODUCTION

Vibrations are fluctuations of a mechanical or structural system about an equilibrium point. Vibrations can be harmful in many situations. Uncontrolled vibration in machinery causes fatigue, damage, loss of function in addition to human-related problems such as discomfort, annoyance, dysfunction, injuries or even disease [1]. Vibration isolators are a solution to this problem. They are applied either to prevent the spreading of vibrational energy from the vibration source, as in engine mounts of vehicles; or to provide protection from vibrational sources, as in seismic isolators of microscopes.

1.1. Objective and Motivation of Study

The main objective of this study is to design a passive self-tuning lever-type vibration isolator. In the absence of damping, lever type vibration isolators have a unique frequency in which they are able to isolate the vibrational energy completely. This is called the antiresonance (zero) frequency of the isolator. The aim of this thesis is to derive a control algorithm and design an associated system which can tune the zero frequency of the isolator to the incoming excitation. This frequency is dependent on the stiffness of the system, the lever ratio and the isolator mass. In this study, adaptivity is achieved by altering the lever ratio of the isolator.

The study consists of three parts. In the first part, the equation of motion for a lever type isolator is derived with a lumped-system analysis. Consequently, the transmissibility and phase difference equations are obtained. Then, a control algorithm utilizing the properties of transmissibility and phase difference is developed. In the second part, the designed control algorithm is tested with multi-body dynamics (MBD) simulations and the control rule is validated. In the final part, the lumped system equations and other idealized properties of the system are replaced with more realistic equations that are based on a distributed parameter model of the system. An experimental set-up for checking the validity of the control rule is developed. The design of each system in the set-up is cultivated by the application of various mechanisms and techniques such as compliant hinges, parallelogram

mechanisms, vibro-impact actuators etc. The set-up is subjected to vibration testing with a shaker and its applicability is validated experimentally.

The literature contains a variety of studies for adaptive or semi-active vibration control. These are dominated by theoretical/experimental work on variable damping and stiffness systems. The application of smart materials and/or electronic control systems is the most popular method in these systems. However, the literature on adaptive lever-type isolators is quite scarce. To the authors' knowledge, there is no passive, mechanical and self-tuning lever type isolator studied before.

1.2. Literature Review

Although vibration may be favorable for some mechanical engineering systems such as conveyors, resonators etc., usually it is detrimental to system performance and is considered as a nuisance. Vibrations induced on vehicles due to road irregularities, vibration induced inaccuracy in precision measuring equipment, buildings subjected to earthquakes and vibration of aircraft wings are some examples where vibration is undesirable.

When vibrations are detrimental, vibration reduction is employed. It can be argued that there are three effective approaches to vibration reduction. The first one is removing/ balancing of the vibration source, the second is vibration absorption and the third is vibration isolation [2]. Removal of the vibration source is outside the scope of this study. Vibration absorption is carried out by adding a secondary system to the point where vibration is to be eliminated, for absorbing and dissipating or storing of vibratory energy. Vibration isolation, as the name implies, is the isolation of vibratory energy by dissipating or reflecting it.

The most widely used vibration absorption systems are the "Auxiliary Mass Systems -AMS". Their development dates back to the beginning of the 20th century when Frahm first patented an AMS in 1911 [3]. The AMS basically consists of an inertia block suspended on a spring of relevant kind. Without damping, they are known as "Dynamic Vibration Absorbers – DVA". If damping is added to the system, 'Tuned Mass Damper – TMD" (or Auxiliary Mass Damper – AMD) is formed. The principle of DVA has given rise to many

applications and is a popular topic in vibration literature. Harris gives a detailed summary of DVA's along with their operating principles and designs [4].

Unlike vibration absorption, vibration isolation involves the isolation of the primary structure. If the vibration source is isolated from other equipment, such as in engines of road vehicles, then it is the primary structure. In this case, the objective is to reduce the forces transmitted from it to the environment. If a body or equipment is isolated from vibration sources, such as in isolation of buildings from earthquakes, then it is the primary structure. For such problems, the isolation objective is to reduce the transmission of displacements. A payload sprung on a spring and damper on the ground is the most basic single degree of freedom (SDOF) isolator. This is a lumped-model approximation to practical isolators and from it, the well-known transmissibility equations are developed. Due to the reciprocity property, both the force and displacement transmissibility equations for this single component isolator are equal [3] and depend on the ratio of isolator's natural frequency to the incoming excitation frequency. In order to isolate a system from excitations at low frequencies, the isolator's natural frequency must be kept even lower than the excitation. It is a well-known fact that the natural frequency of the isolator is related to the ratio of its stiffness to the mass of the payload. Therefore, in order to achieve isolation, either the stiffness of the isolator must be low, or the mass of the system must be high. Increasing mass is applied in some problems such as in vibration reduction of stationary diesel engines and compressors, but this is not a feasible option in many applications in which size or weight constraints are present. Conversely, the stiffness can be reduced but this will increase the displacements of the system under transient motions. Moreover, for vertical systems, such as the suspensions of vehicles, the spring constant can only be decreased to a certain value because the weight of the primary system is also carried by the isolator. In order to overcome this dilemma, engineers in the aerospace industry came up with a solution called dynamic anti – resonant vibration isolator (DAVI) [5]. Developed by Flannelly in the 1960s, the most basic form of anti-resonant vibration isolators use amplification of a relatively small isolator mass by a lever to increase the effective mass of the overall system [6]. This enables DAVI to have a lower ω_n compared to a spring type isolator, even when their stiffnesses and masses are equal. Moreover, due to inertial coupling, an antiresonance frequency is generated at which very high levels of vibration isolation is achieved. Arguably the most common types

of DAVI's are the hydraulic and mechanical types. Hydraulic DAVI's take advantage of hydraulic leveraging principle whereas in mechanical systems a lever and a small isolator mass are used [7].

The mechanical DAVI's can be classified depending on the positioning of the isolator's center of gravity and lever connections to the mass and the base. The two different types of mechanical DAVI's are shown in Figure 1.1. Yilmaz *et al.* describe their properties and equations of motion [8]. Type I isolators have low static displacement whereas Type II isolators offer better lever ratios for the same lever size. In this work, a Type II isolator was studied.

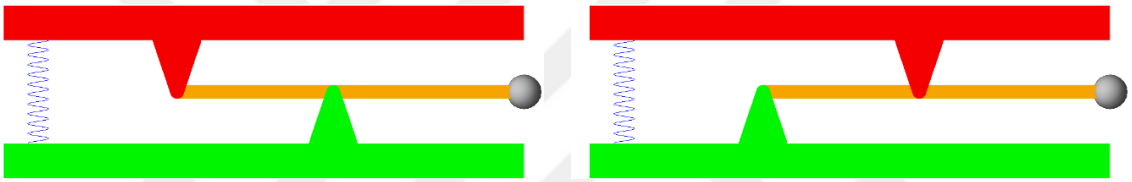


Figure 1.1. Type I (Left) and Type II (right) DAVI

Generally, vibration equipment is similar, i.e. both absorbers and isolators are derivatives of known mechanical equipment such as springs, dampers, levers, etc. However, the difference between vibration absorption and isolation is both in their utilization and point of application. Absorbers are applied at the point where vibration is undesirable, and they absorb the vibration energy at that point. In the case of reactive absorber systems, such as DVA's, they take advantage of anti-resonance frequencies to create a node at their point of application, but they add another degree of freedom (DOF). Therefore, even though the displacement of the primary system becomes zero, two resonances appear in the frequency spectrum. On the other hand, vibration isolators are located in the load path of vibration and reflect or dissipate vibrational energy. For DAVI's, the lever and isolator mass add a zero in the frequency spectrum, but because the lever is connected to both the payload and the base, no additional DOF is introduced. The motion of the isolator is planar with rotation and translation. However, it is known from dynamics that this type of planar motion of a rigid body can be described as a rotation about an instant center of zero velocity. The instant center location is defined by the relative motions of the mass and the base. Following wave-

analogy, this location creates a node at the plane of rotation. At the frequency of maximum isolation, the instantaneous center of zero velocity coincides with the location of the connection of the mass and the isolator. As a result, the payload stays stationary. The interested reader is referred to Yilmaz for more information on DVA's and DAVI's [9].

In practice, DVA's or DAVI's offer a wide variety of opportunities for damping or isolation of vibration. One might choose between the two to satisfy the specific needs of the problem at hand. However, both devices are only applicable to a limited frequency range. Even though this is not a problem for applications involving excitations at constant frequencies, most problems involve vibration induced at a frequency and amplitude unknown beforehand. Moreover, mechanical deterioration and change of working conditions create the risk of de-tuning or even resonance. There are passive devices that can overcome this problem for the vibrations of rotary systems. Pendulum absorbers, ball balancers and pendulum balancers are such adaptive designs that are used to mitigate vibrations stemming from rotational disturbances. Pendulum absorbers benefit from the dependence of pendulum's natural frequency on acceleration field. When these devices are connected to the shaft causing the vibrations, their natural frequency changes along with shaft rotational speed due to centrifugal acceleration. Therefore, as the shaft speed changes, the pendulum's natural frequency follows it [4,10]. Pendulum balancers are used in unbalanced shafts. They adapt themselves to cancel the mass unbalance due to the phase difference of vibrations above a critical speed [11]. Ball balancers also rely on the same principle, but their performance is less than pendulum balancers due to friction and impact observed between balls during operation [12]. Pendulum balancers and absorbers have found applications in the automotive and aerospace industries [10,13].

Non-linear isolators are a common passive solution when excitation frequencies and amplitudes are not known. These devices generally have damping or stiffness constants that are dependent on the amplitude of vibrations. This gives the advantage of a constantly changing natural frequency, thus prevent the excessive growth of vibration amplitudes due to resonance. Arguably, all engineering systems are non-linear, and linearity is only an approximation to their real behaviour. This makes non-linear isolators common in the literature. Narimani *et al.* [14] and Ishida *et al.* [12] studied the effect of piecewise stiffness

and damping coefficients on vibration response. Pranesh *et al.* introduced an earthquake isolator that incorporates a friction pendulum system with amplitude-dependent frequency for civil engineering structures [15]. A common type of non-linear isolators is quasi zero stiffness isolators. In these systems, non-linear springs are utilized to achieve very low stiffness around the operating point. These devices offer very low transmissibility for small displacements about equilibrium. Quasi-zero stiffness devices utilizing Euler-column buckling [16], multi-direction isolators utilizing scissor-like structures [17] and cam structures [18] were created. Another design combines a scissor-like structure with a lever type vibration isolator. The introduced mild nonlinearity enables improvements in the stop bandwidth of the system [19]. Ibrahim gives a review of developments on non – linear vibration isolators up to the year 2008 [20].

Another vibration isolation method takes advantage of the propagation of vibrations as waves in solid structures. These waves can be reflected from point masses or springs connected to beams at wave crests and throughs and the reflected waves can be used to destructively interfere with incoming vibrations. Foda *et al.* inspected the confinement of vibration waves in a Timoshenko beam with reflector masses [21]. This method offers various possibilities for application. Nonetheless, the knowledge of excitation frequency and amplitude are still necessary for its utilization.

All these methods correspond to passive systems, which do not apply control principles to mitigate vibrations. However, the application of passive methods requires the knowledge or estimation of working conditions at the design stage. Even though such knowledge may be present, passive systems may not always provide enough vibration mitigation due to changing conditions (i.e, changing excitation frequency and/or amplitudes). As a countermeasure, principles of control theory are utilized. The approach to vibration reduction can be classified as passive, active or semi-active depending on the amount of power required in the control action. Passive systems require no energy input for operation, active systems utilize control to the full extent so have high energy requirement and semi-active devices are in between the two.

Active systems utilize the destructive interference property of waves for vibration attenuation [22]. They are utilized in various industries such as the aerospace, automotive, precision equipment etc. Despite the high amounts of vibration reduction possible, they generally require power sources, actuators, sensors and other complicated electronic equipment, rendering them either too expensive or too complicated for many practical applications. The required force and energy magnitudes make their use nearly impossible in massive structures such as buildings, bridges, vehicles etc. Moreover, there are issues with stability due to external energy input to the system [23]. Nakano *et al.* studied regenerative systems for active isolation, but such systems require additional energy regeneration and storing equipment, and it is not possible to achieve total vibration isolation with regenerated energy [24].

Semi-active systems have the stability of passive systems along with the adaptability of active systems. The idea behind the semi-active control is to alter the properties of system components such as damping, stiffness or mass in order to achieve a high level of vibration isolation. This generally requires small actuators and the power requirements are orders of magnitude lower than active systems. Karnopp gives a comparison of active and semi-active control techniques along with a historical description of the subject [25]. The initial studies on semi-active vibration control were aimed toward dampers for suspensions of vehicles [26]. Later, other control concepts were developed and semi-active damping systems were improved for other fields such as in civil structures [27]. Developments in actuator systems and smart materials increased the range of possibilities and applications [28–35]. The feasibility of semi-active control concept enables its use in both vibration absorbers and vibration isolators.

In the absence of damping, AMS's offer vibration reduction in a very narrow frequency band. What's more, they add two resonance frequencies to the FRF. This makes their utilization difficult and even dangerous for various practical applications. In order to increase their feasibility, adaptive systems are utilized [36]. The anti-resonance frequency of AMS's depend on their spring constant. Acar and Yilmaz used a tension string-mass system whose natural frequency is controlled by the tension in the string that is altered via a negative stiffness – electric motor system [37]. Walsh and Lamancusa inspected the - gearset

[38]. Piezoelectric materials shunted with a variable inductive circuit [39] are another group of variable frequency vibration absorbers. There are also patented designs for variable stiffness utilizing pneumatic springs [40] or mechanical tuning of elastomeric mounts[41]. Another group of researchers studied the effect of changing inertance in vibration absorbers. The application of a rotational type inerter whose inertance was varied with a continuously variable transmission (CVT) in parallel with a spring in a DVA was researched by Brzeski *et al.* [42,43]. They showed that the effect of non-linearities of the actual system is minimal. The final group is the variable damping TMDs. Studies were conducted to maximize the performance of semi-active TMDs controlled by variable dampers [44–46].

The application of semi-active devices for vibration isolation started with vehicle dampers [26]. In these initial studies, the control approach was directed towards developing a semi-active damper such that its effect could simulate that of a damper which was connected to the payload and the ground of an inertial frame. For this purpose, a control rule which alters the damping between a high and low value in a vibration cycle called the sky-hook control scheme was created [47]. Later, other control schemes were developed [27,48,49]. Simultaneously, various designs were developed for the variable damper concept. Karnopp gives the description of an electrical, hydraulic and electromagnetically controlled friction damper and how electromechanical analogies can be used to construct analogue devices with different energy domains [50]. Applications of electrorheological and magnetorheological materials are also commonly researched [27,51]. Because the weight of the structure is generally carried by the isolator, utilization of variable stiffness devices is more complicated than variable damping. Even so, variable stiffness was researched for various systems, such as transverse vibration supports. Variable stiffness can be obtained with the application of a geometric non-linearity [52]. Another common concept is the application of magnetorheological elastomers (MREs) [53,54].

In most of the semi-active systems, electronic equipment such as sensors, controllers, logic circuits and power sources are required. Even though the power requirements are lower than active systems, power consumption by these systems is not desirable in some applications. Therefore, self-sensing stiffness [55] or self-powered damper [56,57] elements were considered in different studies. Another group of self-powered vibration mitigation

devices use piezoelectric shunt-damping circuits and alter its properties with electrical switches to dissipate the vibration energy [58]. Their mechanical analogues serial-switched stiffness systems (SSSS) use mechanical switches to change spring constant in time scales an order of magnitude lower than the excitation periods [59]. These systems alter the stiffness properties during a cycle, so they attenuate the potential energy in the form of kinetic energy. In that sense, these methods are similar to the described semi-active control schemes for dampers such as skyhook, ground hook, etc. They can be tailored to be self-powered, but the tuning effect is not permanent; when the control forces are removed, the system returns to the initial configuration. Therefore, the control action is required for all vibration cycles.

The literature on semi-active control of DAVI's is relatively limited. Du Plooy *et al.* designed and experimentally validated an adaptive hydraulic type DAVI. The anti-resonance frequency was altered by a pneumatic spring which was controlled with an electronic valve [60]. A recent patent by Bueter et al. describes a semi-active system for a lever-type DAVI [61]. However, the patent is focused on actuator concepts applicable to the system.

All the studies mentioned rely on electronic circuits and sensors for control action. There are patents on fully mechanical self-tuning DVA's which adapt to the excitation frequency by utilizing phase differences between components in the system [62,63], but there is no data on the performance of these systems. To the best of author's knowledge, there is no work done on adaptive self-tuning lever-type vibration isolators that are fully mechanical (no use of electronic sensors, controllers or actuators). In this study, an adaptive lever-type DAVI which employs mechanical means to tune itself with no external energy was developed. In order to achieve self-sensing actuation with vibratory energy, a vibro-impact actuator was used. Vibro-impact type systems are common in ultrasonic motors. Sashida *et al* and Ragulskis *et al.* describe the structure and operating principles for such systems [64,65].

1.3. Overview of Thesis

The first chapter of this thesis focuses on the introduction of the subject, the motivation, the significance of the study, and a brief description of the development of the subject with similar notable studies from the literature. In the second chapter, the equations of motion for the lever type DAVI's are derived and used to develop the control algorithm. In the third chapter, this algorithm is validated with numerical MBD simulations. Chapter 4 describes the design of the experimental set-up. In chapter 5, experimental results are shown. In the final chapter, a brief summary and conclusions are presented.

2. THE DEVELOPMENT OF THE CONTROL ALGORITHM

2.1. Lumped Model Equations for Type II Lever Type DAVI

Consider the lumped parameter model of Type II lever-type isolator in Figure 2.1. Here, the lever is massless, rigid and there is no damping in the system. The length of the lever is l_1, the hinge spacing is l_2 and the lever makes an angle θ with the horizontal. The displacements of the base, payload mass and the lever tip are denoted as y_1, y_2 and y_3, respectively. Assuming a sinusoidal excitation coming from the base and θ is small, y_3 can be obtained in terms of y_1 and y_2:

$$y_3 = \alpha y_2 - (\alpha - 1)y_1 \quad where \ \alpha = \frac{l_1}{l_2} > 1 \tag{2.1}$$

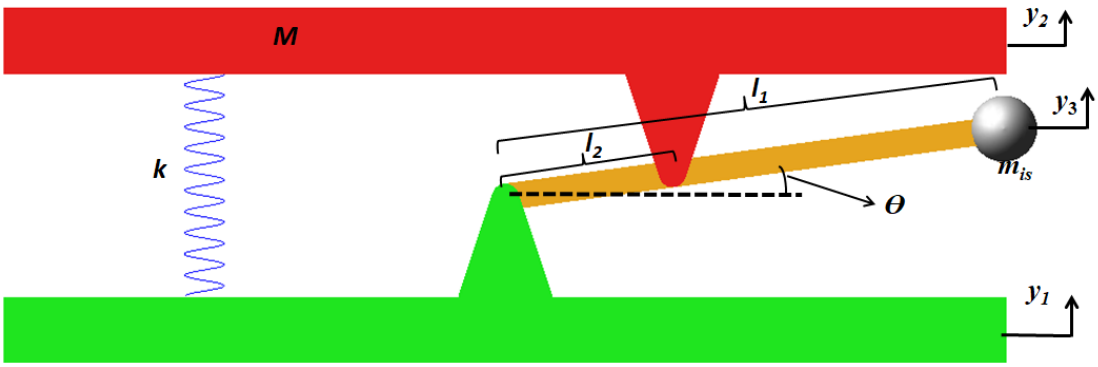


Figure 2.1. Lumped parameter model of the lever-type isolator

Using Equation 2.1, the kinetic energy T is obtained as:

$$T = \frac{1}{2}M\dot{y}_2{}^2 + \frac{1}{2}m_{is}[\alpha y_2 - (\alpha - 1)y_1]^2 \tag{2.2}$$

Similarly, the potential energy of the system can be obtained as follows:

$$V = \frac{1}{2}k(y_2 - y_1)^2 \tag{2.3}$$

The Lagrange equation is:

$$\frac{d}{dt}\left(\frac{\delta T}{\delta \dot{q}_k}\right) - \frac{\delta T}{\delta q_k} + \frac{\delta V}{\delta q_k} = Q_k \tag{2.4}$$

Substituting Equation 2.2 and Equation 2.3 into Equation 2.4 in the absence of damping, the equation of motion can be obtained as follows:

$$(1 + \mu\alpha^2)\ddot{y}_2 + {\omega_0}^2 y_2 = \mu(\alpha^2 - \alpha)\ddot{y}_1 + {\omega_0}^2 y_1 \tag{2.5}$$

where

$$\mu = \frac{m_{is}}{M}, \qquad \omega_0 = \sqrt{\frac{k}{M}} \tag{2.6}$$

For a periodic input to the system in the form of $y_1 = Y_1 e^{i\omega t}$, a periodic solution of the form $y_2 = Y_2 e^{i\omega t}$ is assumed:

$$[{\omega_0}^2 - \omega^2(1 + \mu\alpha^2)]Y_2 = [{\omega_0}^2 - \omega^2\mu(\alpha^2 - \alpha)]Y_1 \tag{2.7}$$

From Equation 2.7, the resonance (pole) frequency ω_p is:

$$\omega_p = \sqrt{\frac{{\omega_0}^2}{(1+\mu\alpha^2)}} \tag{2.8}$$

The antiresonance (zero) frequency ω_z is:

$$\omega_z = \sqrt{\frac{{\omega_0}^2}{\mu\alpha(\alpha-1)}} \tag{2.9}$$

The transmissibility can be obtained by using Equation 2.8 and Equation 2.9 as;

$$Tr(\omega) = \frac{Y_2}{Y_1} = \frac{(1-\omega^2/{\omega_z}^2)}{\left(1-\omega^2/{\omega_p}^2\right)} \tag{2.10}$$

The phase angle is:

$$\phi = \begin{cases} 0, & \omega < \omega_p \\ \pi, & \omega_p < \omega < \omega_z \\ 0, & \omega_z < \omega \end{cases} \tag{2.11}$$

Using Equation 2.10 and Equation 2.11, the transmissibility and phase angle plots for a representative lever-type isolator are obtained in Figure 2.2.

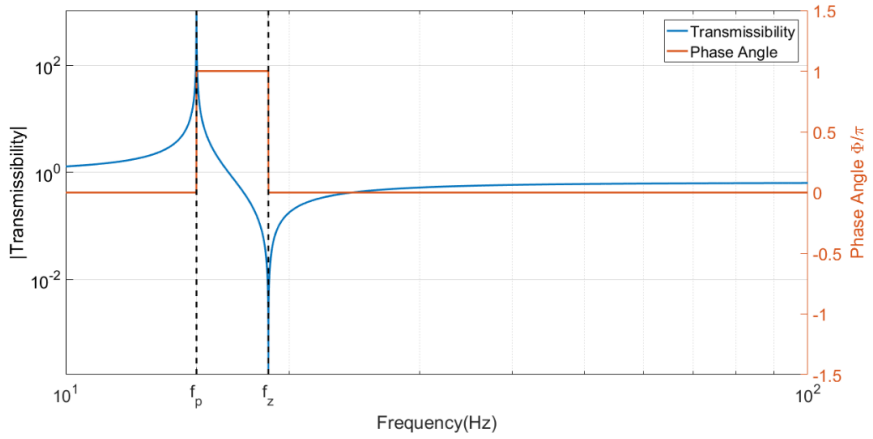


Figure 2.2. The transmissibility and phase angle plot of a lever type vibration isolator with f_p=15 Hz, f_z=18.75 Hz, μ=0.1, α=5.82 where $\omega_p = 2\pi f_p$ and $\omega_z = 2\pi f_z$.

2.2. The Development of the Control Algorithm

Inspection of Figure 2.2 highlights the following 5 cases (3 frequency ranges separated by ω_p and ω_z):

- $\omega < \omega_p < \omega_z$: For this range, $|Y_2| > |Y_1|$, the phase angle is 0, hence the base and the mass move in-phase.
- $\omega = \omega_p < \omega_z$: At the resonance frequency, $Y_2 \to \infty$.
- $\omega_p < \omega < \omega_z$: For this range, the phase angle is π, hence the base and the mass move out-of-phase.
- $\omega_p < \omega = \omega_z$: At the antiresonance frequency, $Y_2 = 0$.
- $\omega_p < \omega_z < \omega$: For this range, $|Y_1| > |Y_2|$, the phase angle is 0, hence the base and the mass move in-phase.

Because of the small θ assumption, the motion of all points on the lever, e.g. the base-hinge, the mass-hinge and the isolator are sinusoidal about an equilibrium for sinusoidal excitation. For a given excitation amplitude and frequency, their amplitudes and phases are known, and are given by Equation 2.10 and Equation 2.11. The motion of the lever is that of a rotation and a translation at the same plane. It is known from dynamics that planar motion of rigid bodies can be described as a rotation about an instantaneous center of zero velocity

if it is not a pure translation (for pure translation the instant center can be assumed at the infinity). For many accelerating systems, the instantaneous center of zero velocity changes rapidly, hence the name 'instantaneous'. However, for the present problem, all the velocities, displacements and accelerations are proportional due to the sinusoidal nature of motion. The ratio of the velocity of the mass hinge and base hinge, as well as the ratio of their displacement and acceleration, is a function of excitation frequency and is given by the transmissibility (Equation 2.10) and phase angle (Equation 2.11) equations. As a result, for constant frequency, the location of the instant center of zero velocity stays stationary during the course of a vibration cycle. Instantaneous center of zero velocity position is described below for the mentioned five frequency ranges:

- $\omega < \omega_p < \omega_z$: The instant center is located towards the left of the base hinge.
- $\omega = \omega_p < \omega_z$: This is the resonance condition and the instant center is on the base hinge.
- $\omega_p < \omega < \omega_z$: The instant center is between the mass hinge and the base hinge.
- $\omega_p < \omega = \omega_z$: This is the antiresonance condition and the instant center is on the mass hinge.
- $\omega_p < \omega_z < \omega$: The instant center is located towards the right of the mass hinge.

The instant center locations can be better visualized with MBD simulations. The visualization of system elements' superposed motion observed from a stationary reference obtained with MSC Adams are shown in Figure 2.3 to Figure 2.7. The location of the instant center of zero velocity for the lever bar is marked with a red circle in each figure. It can be observed that its location is a monotonic function of ω and moves to the right (to the left if the isolator is directed towards left) as the frequency increases. Referring to wave analogy, it can be stated that the lever has a nodal point whose position depends on the excitation frequency. Therefore, displacement of the payload mass will be zero if the location of its hinge coincides with this nodal point as in case 4 (see Figure 2.6). This case corresponds to perfect vibration isolation.

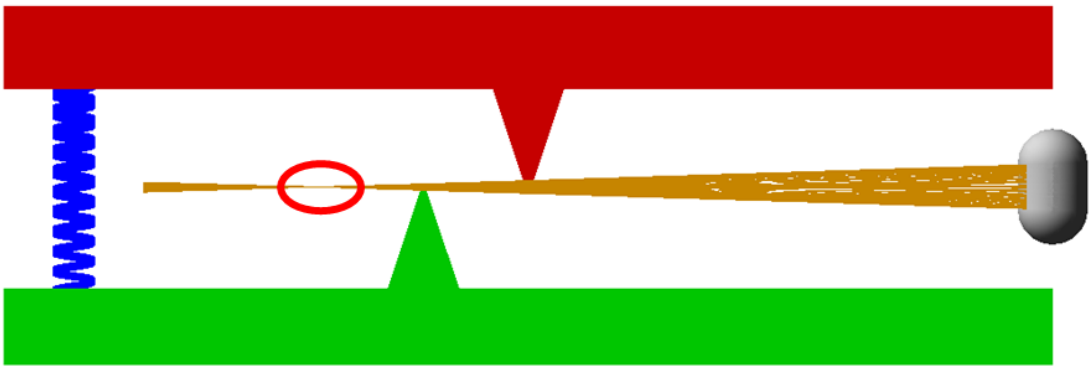


Figure 2.3. Case1: Motion of the system for $\omega < \omega_p < \omega_z$. Here, $|Y_2| > |Y_1|$

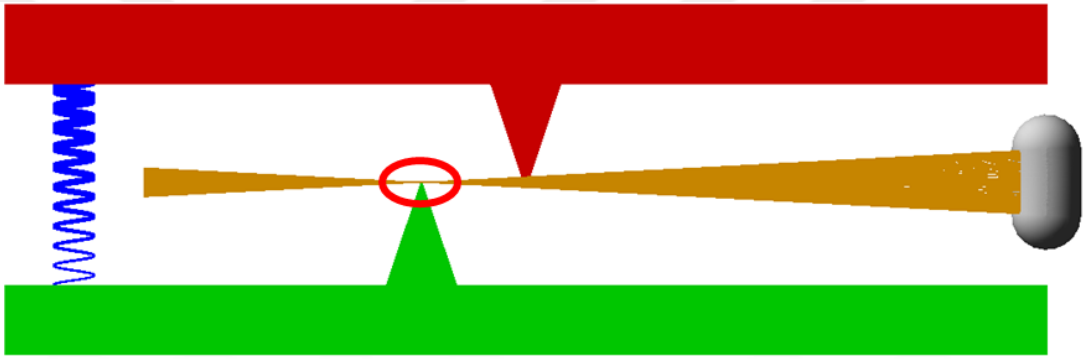


Figure 2.4. Case 2: Motion of the system for $\omega = \omega_p < \omega_z$. Here, $Y_2 \to \infty$

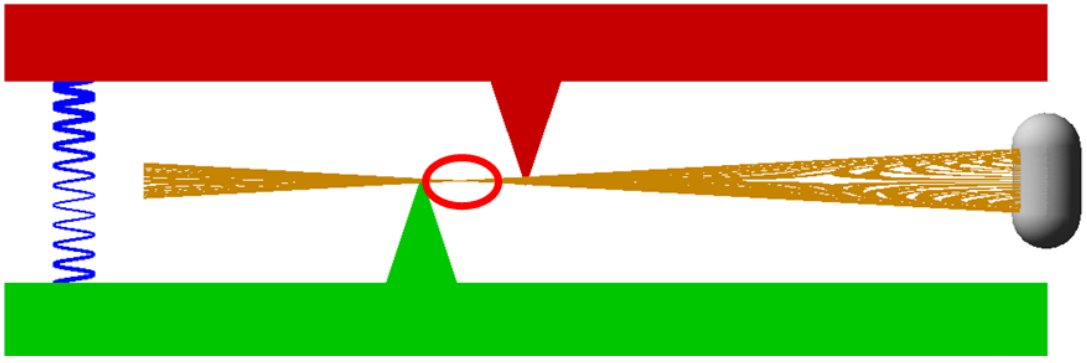


Figure 2.5. Case 3: Motion of the system for $\omega_p < \omega < \omega_z$

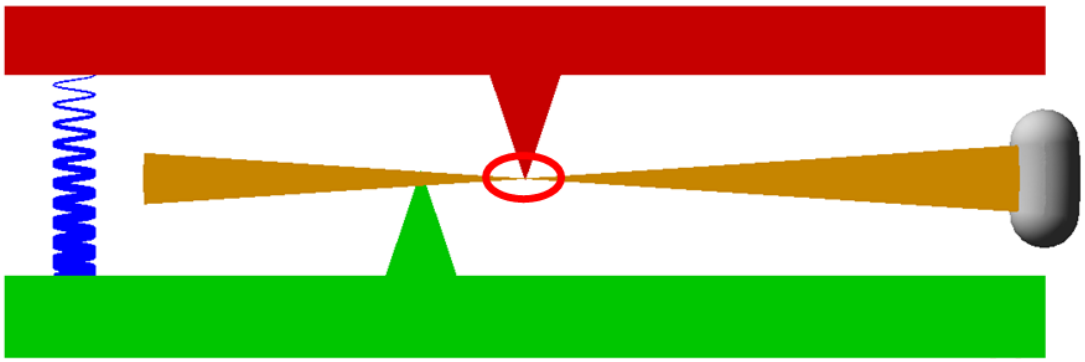


Figure 2.6. Case 4: Motion of the system for $\omega_p < \omega = \omega_z$. Here, $Y_2 = 0$

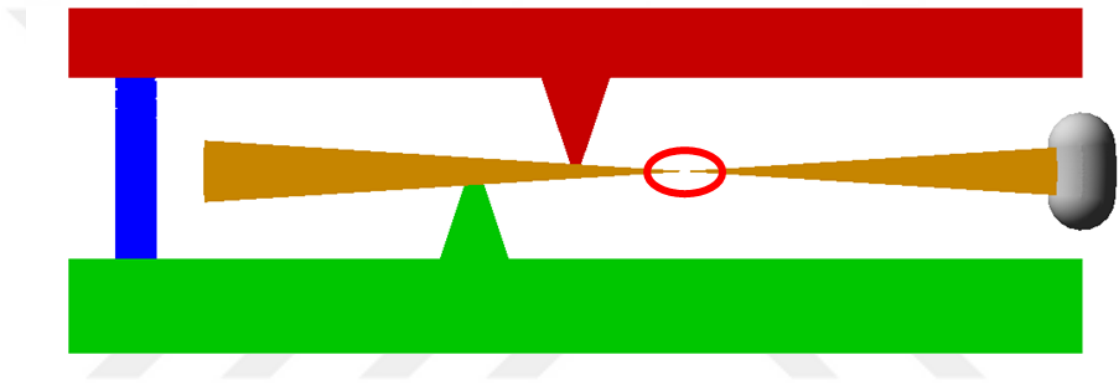


Figure 2.7. Case 5: Motion of the system for $\omega_p < \omega_z < \omega$. Here, $|Y_1| > |Y_2|$

Assume that the hinge spacing (l_2) is fixed and the lever length (l_1) is to be determined to obtain the antiresonance condition (case 4). By using α in Equation 2.9 and assuming positive frequencies (ω>0), l_1 for this perfect isolation case can be obtained as:

$$l_1(\omega) = l_2\left[1 + \sqrt{1 + \frac{4{\omega_n}^2}{\mu\omega^2}}\right] \tag{2.12}$$

One can see that if the lever length can be changed as the excitation frequency changes, the system will always remain in antiresonance condition. As a result, the output vibration amplitude (Y_2) will be zero for all the frequencies in the operation range.

To achieve this aim, a novel system is designed (see Figure 2.8) in which a lever of constant length is used. The effective lever length is l_1, and the distance between the two

hinges is l_2, giving the lever ratio as l_1/l_2 (Figure 2.8(a)). Assume that the velocity amplitude is measured at two equidistant locations from the mass hinge and forces that are proportional to the velocity amplitudes are applied in opposite directions (see Figure 2.8(b)). Calling the force pulling to the left as F_1 and to the right as F_2, the lever will slide to the direction of the left for $F_1>F_2$ and to the right for $F_2>F_1$. Because the forces are proportional to velocity, the larger force is further away from the instant center location. The tuning action requires bringing the mass hinge closer to the instant center location. Thinking in relative terms, moving the isolator (in the opposite direction we want to move the mass hinge) will provide the same effect. In cases 1, 2 and 3, the right force will be greater than the left force as the lever experiences higher velocity amplitude at the right measurement point (as seen in Figure 2.8(b)). The instant center is to the left of the mass hinge, so it must move left. Keeping it stationary, the lever will be moved right. Thus, the instant center will move to the right, as well. When the instant center meets the payload hinge point, then both forces will be equal, and the lever will not move horizontally anymore, and it will just oscillate in this antiresonance condition. Hence, cases 1, 2 and 3 will eventually converge to case 4.

On the other hand, in case 5, the left force will be greater than the right force as the lever experiences higher amplitude at the left measurement point. Consequently, the lever will move to the left as it oscillates. Thus, the instant center will move to the left, as well. When the instant center meets the payload hinge point, then both forces will be equal, and the lever will not move horizontally anymore, and it will just oscillate in this antiresonance condition.

In summary, all cases will converge to case 4 and perfect vibration isolation will be achieved due to the antiresonance condition. This is a consequence of the monotonic relation of instant center location and the excitation frequency. As the tuning operation proceeds, no inflection points are passed, so a proportional control algorithm in which two sensors and two actuators are used is sufficient for self-tuning operation

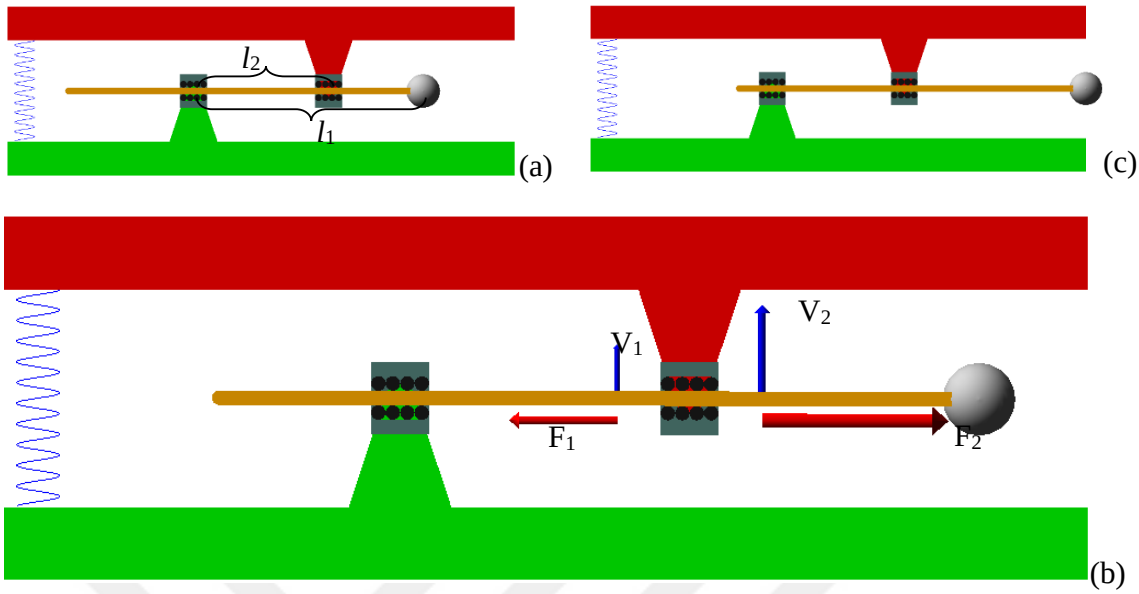


Figure 2.8. Self-tuning operation of the lever (a) start, (b) progress (c) tuned system

This algorithm can be implemented by using two vibro-impact type mechanical actuators that produce opposing control forces that are proportional to the vibration amplitude. These two actuators will work at the same time. If the two control forces are equal in magnitude, then the net force on the lever will be zero and the lever ratio remains the same. If one actuator experiences higher vibration, then it will generate a higher force and push the lever towards its side. Consequently, the lever ratio will change so as to change the antiresonance frequency to match the excitation frequency. Here, it is assumed that the excitation frequency is constant, and the system changes the lever ratio to bring the antiresonance frequency to the level of the excitation frequency.

The algorithm is described in Figure 2.9.

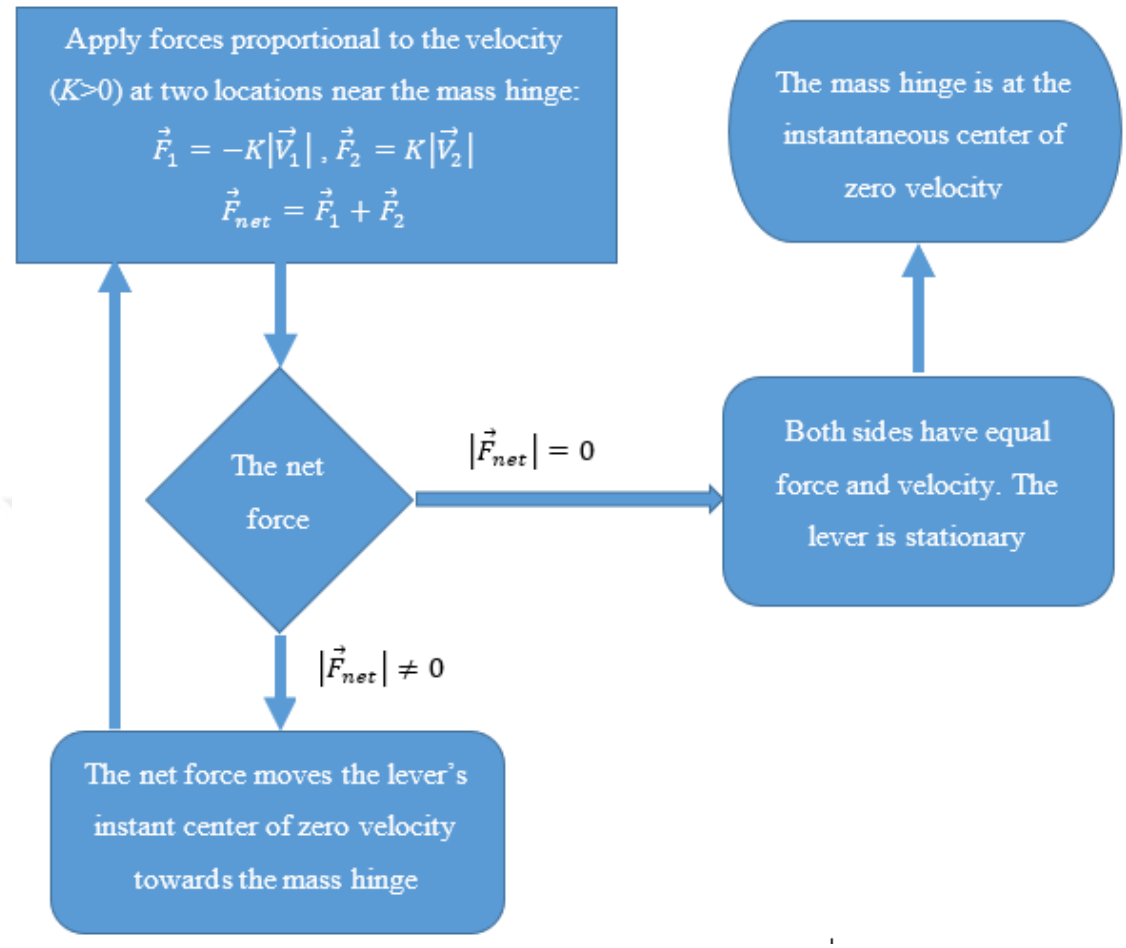


Figure 2.9. Flowchart of the control algorithm

3. NUMERICAL VERIFICATION

In this part, the control algorithm is verified with MBD simulations in MSC Adams. In chapter 2, an excitation from the base is applied to the lumped parameter system in which the lever is massless and the isolator mass is a point mass connected to its end. Two locations are selected on the lever, with equal distance from the mass hinge. Two forces are defined, proportional to the velocity of these two locations, pulling the lever in their direction, as in Figure 3.1.

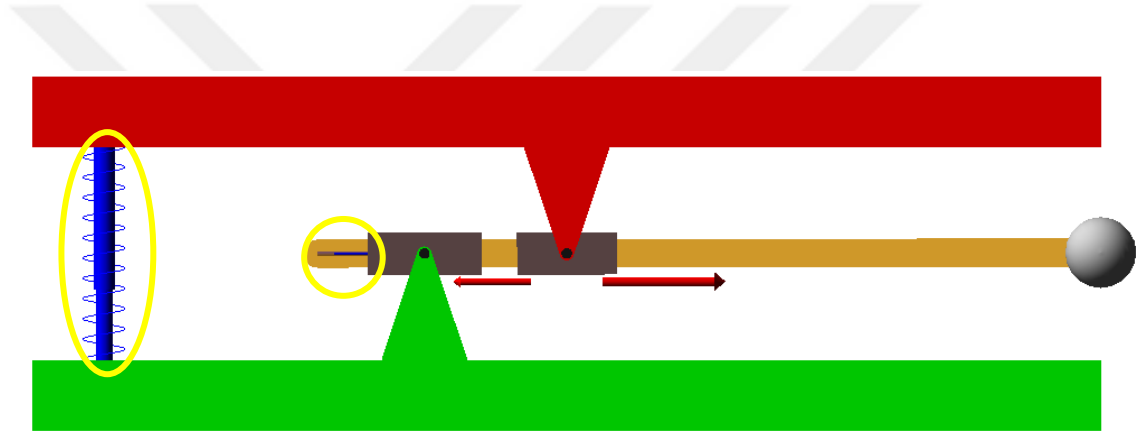


Figure 3.1. The representative system and locations of the dampers (marked with yellow curves) and forces (shown in red under the lever)

In order to provide a variable lever ratio in simulation, two links are defined at the mass and base hinges, connected to the corresponding bodies with revolute joints (shown in brown in Figure 3.1). The lever and isolator mass are connected to these links with telescopic joints. In one of the telescopic connections, a small friction force is defined. The application of this friction force is necessary because of the centrifugal force of the isolator and lever. This force is overlooked in the derivation of equations due to the small angle assumption. For a system with a fixed lever ratio, its effects are small and can be neglected. Moreover, the lever is constrained to the mass and base at the hinges, so no DOF is present in its direction. However, for this problem, the lever is able to move in the horizontal direction as well. This creates a force in the direction of this new DOF and can cause unrestrained motion of the lever. Its magnitude can be obtained as follows:

$$\left|F_{centrifugal}\right| = m_{is}[\ddot{y}_2 \sin(\theta) - (l_1 - l_2)\dot{\theta}^2] \tag{3.1}$$

Notice that θ and its derivatives are obtained as below due to small angle assumption:

$$\theta \cong \frac{y_2 - y_1}{l_2}, \dot{\theta} = \frac{\dot{y}_2 - \dot{y}_1}{l_2} \tag{3.2}$$

Inspection of Equation 3.1 and Equation 3.2 and considering Equation 2.10, it can be observed that $F_{centrifugal}$ is a function of excitation amplitude and frequency. Because it is hard to predict it for all situations, a pre-determined friction force preload is applied to one of the telescopic joints. Note that this force will prevent the described tuning action after the net tuning force is less than its magnitude, namely:

$$\left|F_{friction}\right| > \left||F_1| - |F_2|\right| \tag{3.3}$$

Therefore, $\left|F_{friction}\right|$ is kept as low as possible. Its magnitude is less than 2% of F_1 and F_2 in all simulations. In addition to friction, dampers are applied both at the main spring (connecting mass and base) and the lever as shown in Figure 3.1. The application of damping is necessary because the tuning action during vibration creates harmonics in the system. In the absence of damping, these harmonics cannot be attenuated. Moreover, the tuning action itself requires damping. If the system is excited at frequencies close to resonance, excessive velocities are created in the lever. As a result, huge control forces will be created. In the absence of damping, this creates a huge overshoot and possible divergence risk. Another possible problem is the back and forth motion of the lever. Such motion can be triggered by the control forces and if no damping is applied, this creates an artificial damping in the isolator which is detrimental to system performance. Therefore, empirically selected damping with overall damping ratio ξ of 0.013 is applied in the simulations.

The system's FRF at the initial position is given in Figure 3.2. The simulations start from this initial condition with five distinct excitation frequencies with the same motion

amplitude. These frequencies correspond to the cases described in Chapter 2. They are shown with blue dashed lines in Figure 3.2.

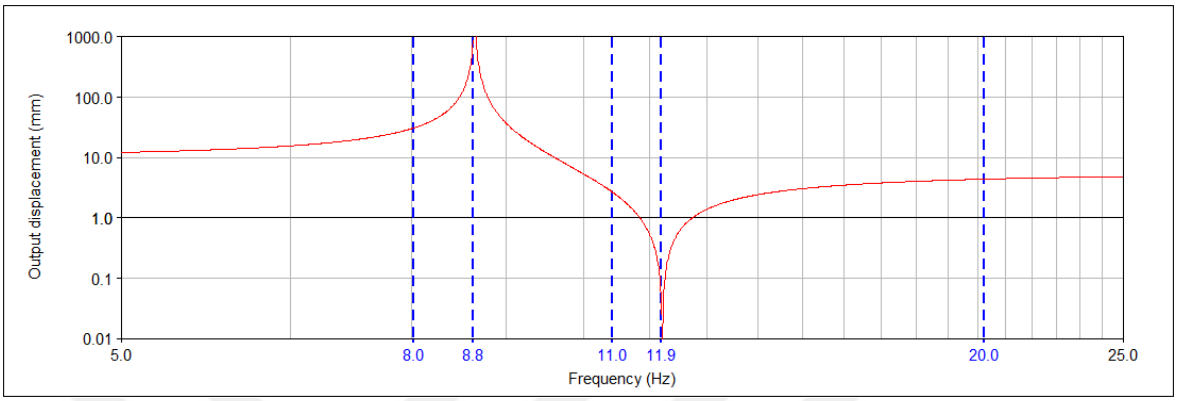


Figure 3.2. The selected frequencies (blue dashed lines) shown on the FRF plot of the system for amplitude

In order to observe the effectiveness of the algorithm, time plots of the payload mass displacement and the lever displacement are created for all simulations (Figure 3.3 to Figure 3.7). In all cases, the input vibration amplitude is constant (0.1mm). Because the properties of the model are arbitrary (mass, stiffness, amplitude etc.), normalized plots are created. The motion of the mass is normalized by the input excitation amplitude Y_1 and the motion of the lever is shown by the change in the ratio of the lever length to distance between the hinges l_2, giving the lever ratio α defined in Equation 2.1. At the initial situation, the lever ratio is the same (4.75) for all five cases, marked with dash lines in plots. However, different behaviour is observed in each frequency, so the plot scale for α is different in all plots. Similarly, for the normalized mass displacement, excessive values are observed in the first two frequencies. Therefore, the plot scale is larger in the first two plots compared to the last three.

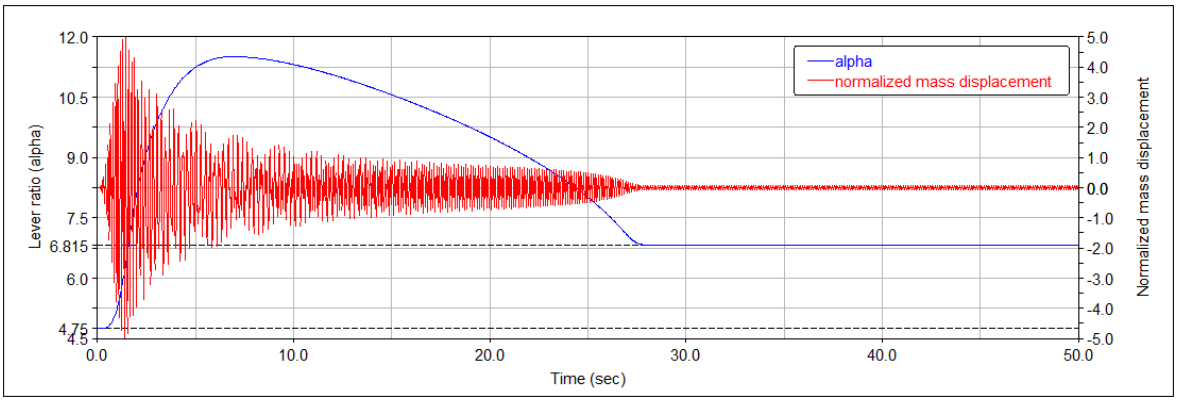


Figure 3.3. Time response for $\omega = 8$ Hz , i.e., $\omega < \omega_p < \omega_z$

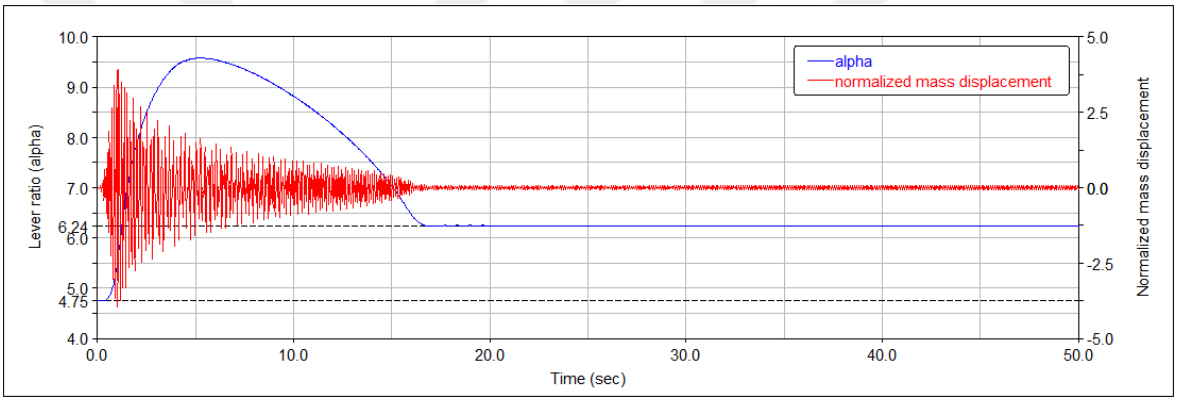


Figure 3.4. Time response for $\omega = 8.8$ Hz , i.e., $\omega = \omega_p < \omega_z$

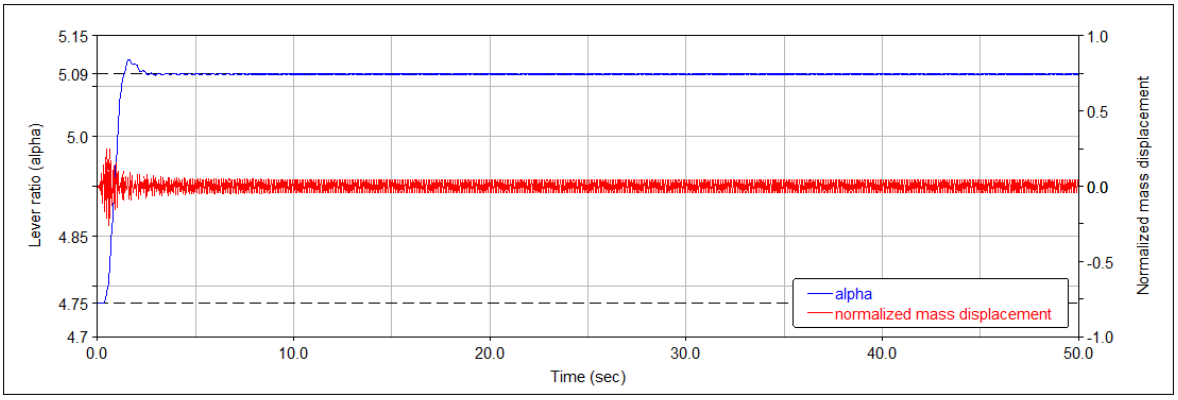


Figure 3.5. Time response for $\omega = 11$ Hz , i.e., $\omega_p < \omega < \omega_z$

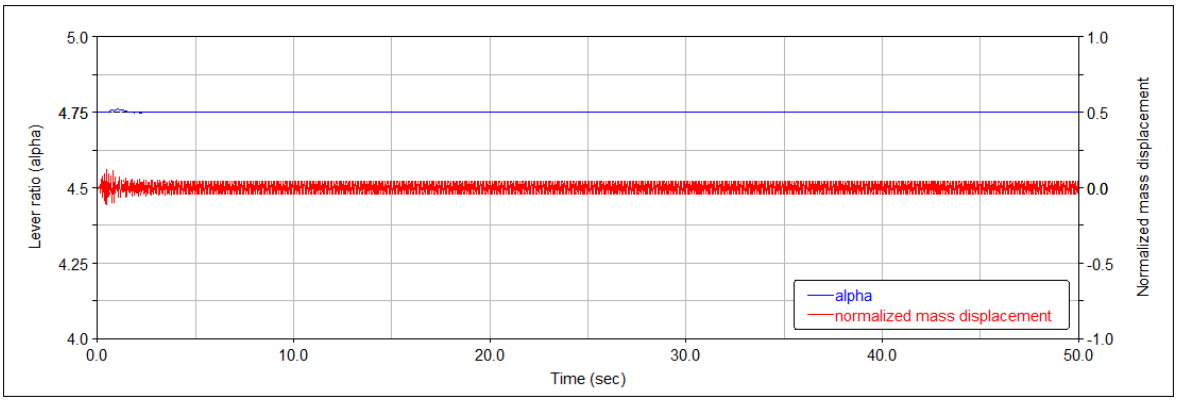


Figure 3.6. Time response for $\omega = 11.9$ Hz , i.e., $\omega_p < \omega = \omega_z$

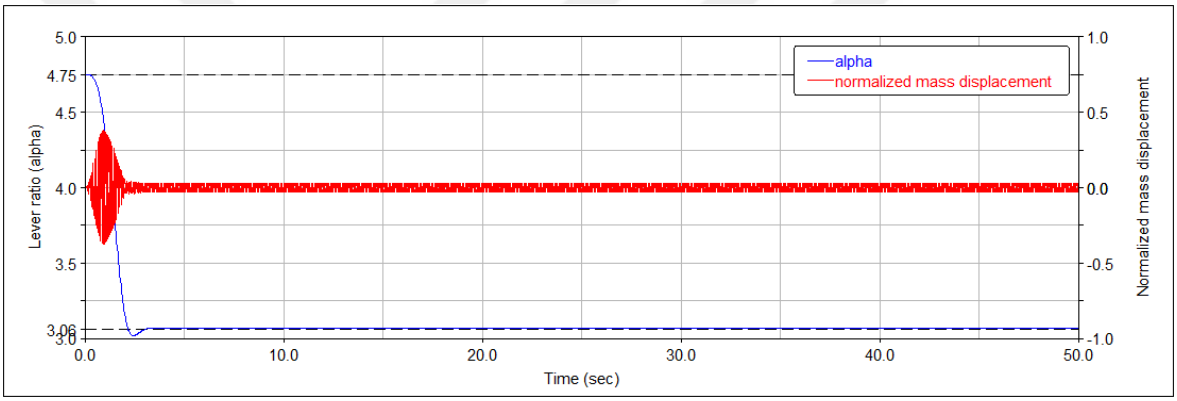


Figure 3.7. Time response for $\omega = 20$ Hz , i.e., $\omega_p < \omega_z < \omega$

Comparison of the five simulations shows that the displacement amplitude of mass in the first two simulations is larger than the rest. This is because the system passes through resonance in these two simulations. For a system such as the one shown in Figure 3.1, in which the base hinge is to the left and the mass hinge is to the right; the instant center location of the lever lies to the left of the base hinge for frequencies less than ω_p. As the tuning action proceeds, its location moves towards the right-hand side (RHS), until it passes through the base hinge. However, as explained in Chapter 2, this corresponds to the resonance condition (see Figure 2.4). As a result, the system shows excessive values before falling to smaller values. This behaviour is clearly visible in mass displacements and is also observable in α. For the latter case, the excessive lever velocities observed while passing through resonance creates a huge overshoot, which is recovered after.

Simulation results reveal that the control algorithm enables the reduction of vibration for all cases. Theoretically, in all the plots output displacement should have converged to zero. However, as shown in Equation 3.3, the friction used in the model prevents the movement of the lever below small values of the net force. When the instant center of zero velocity gets close to the mass hinge, the difference between RHS and left-hand side (LHS) velocity becomes small. After some point, its magnitude falls below the friction force, and the tuning action stops. Another detrimental effect is the damping in the system. The presence of damping reduces the performance of DAVI's and increases the transmissibility, resulting in higher mass displacement amplitudes. Hence, a small amount of damping is used in the system.

4. THE DESIGN OF EXPERIMENTAL SET-UP

4.1. Distributed Parameter Model

The equations so far were derived assuming the system consists of lumped masses and massless levers acting as rigid bodies. However, it is very hard to realize massless lever approximation in real systems. To benefit from the isolation effect of a lever, its first natural frequency must be higher than the working frequencies, so that it can be considered as a rigid body. In order to realize this, the lever's area moment in the longitudinal cross-section must be kept higher than some threshold value. This makes the lever mass comparable to the isolator mass. As a result, the mass and mass moment of inertia of the lever are not negligible, so the resonance and antiresonance frequencies of the system should be revised, accordingly.

In Figure 4.1, new variables are introduced to include the effects of the mass and mass moment of inertia of the lever to the equation of motion of the system.

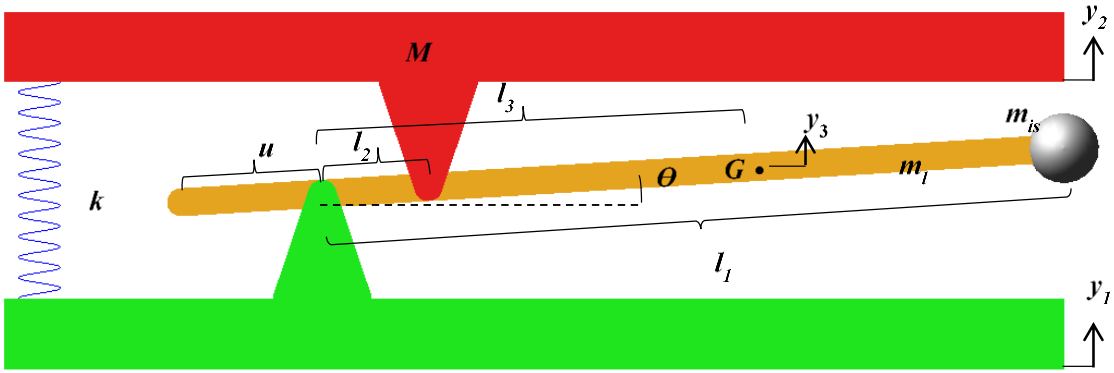


Figure 4.1. The variables used in the prototype system.

In this configuration, G is the location of the center of mass, l_3 is the distance between the base hinge and G, l_1 is the lever length between the base hinge and isolator mass, l_2 is the distance between two hinges, u is the distance between left lever tip and base hinge, m_l is the lever mass, m_{is} is the isolator mass, y_3 is the displacement of G in the vertical direction,

θ is the angle the lever makes with horizontal, *k* and *M* are spring constant and payload mass, respectively.

Assuming small θ, the displacement of the center of mass G in terms of y_1 and y_2 is:

$$y_3 = \beta y_2 + (1-\beta) y_1 \; where \; \beta = \frac{l_3}{l_2} \tag{4.1}$$

The kinetic energy of the system is:

$$T = \frac{1}{2} M \dot{y_2}^2 + \frac{1}{2} I_z \frac{\alpha^2}{{l_1}^2} (\dot{y}_1 - \dot{y}_2)^2 + \frac{1}{2} (m_{is} + m_l)(\beta \dot{y}_2 + (1-\beta)\dot{y}_1)^2 \, , \alpha = \frac{l_1}{l_2} \tag{4.2}$$

Assuming the isolator mass is a point mass, the location of G can be calculated as:

$$l_3 = \left(\frac{2m_{is} + m_l}{m_{is} + m_l}\right)\left(\frac{l_1 + u}{2}\right) - u \tag{4.3}$$

Similarly, the moment of inertia in the out-of-plane axis is as follows:

$$I_z = \frac{1}{12} m_l (l_1 + u)^2 + m_l (\frac{(u - l_1)}{2} + l_3)^2 + m_{is}(l_1 - l_3)^2 \tag{4.4}$$

The potential energy of the system is:

$$V = \frac{1}{2} k (y_2 - y_1)^2 \tag{4.5}$$

The Lagrange equation for the undamped case is:

$$\frac{d}{dt}\left(\frac{\partial T}{\partial \dot{y}_2}\right) + \frac{\partial V}{\partial y_2} = 0 \tag{4.6}$$

The equation of motion can be obtained for y_2 using Equation 4.6 with Equation 4.5 and Equation 4.2:

$$\left[M + I_z \frac{\alpha^2}{{l_1}^2} + (m_l + m_{is})\beta^2\right]\ddot{y}_2 + ky_2 = \left[(m_{is} + m_l)\beta(\beta - 1) + I_z \frac{\alpha^2}{{l_1}^2}\right]\ddot{y}_1 + ky_1 \tag{4.7}$$

From the LHS of Equation 4.7, the resonance frequency of the system can be obtained as follows:

$$\omega_p = \sqrt{\frac{k}{M + I_z \frac{\alpha^2}{{l_1}^2} + (m_l + m_{is})\beta^2}} \tag{4.8}$$

Similarly, the anti-resonance frequency of the system can be obtained from the RHS of Equation 4.7:

$$\omega_z = \sqrt{\frac{k}{(m_{is} + m_l)\beta(\beta - 1) + I_z \frac{\alpha^2}{{l_1}^2}}} \tag{4.9}$$

4.2. The Design of the Prototype System

In addition to the numerical verification presented in Chapter 3, experimental validation is also carried out. In this part, the design of a prototype DAVI with an adjustable lever ratio is presented. The realization of various features of idealized systems such as the hinges, the springs and the telescopic joints are carried out with custom made replacements. The 3-D model of the set-up is shown in Figure 4.2.

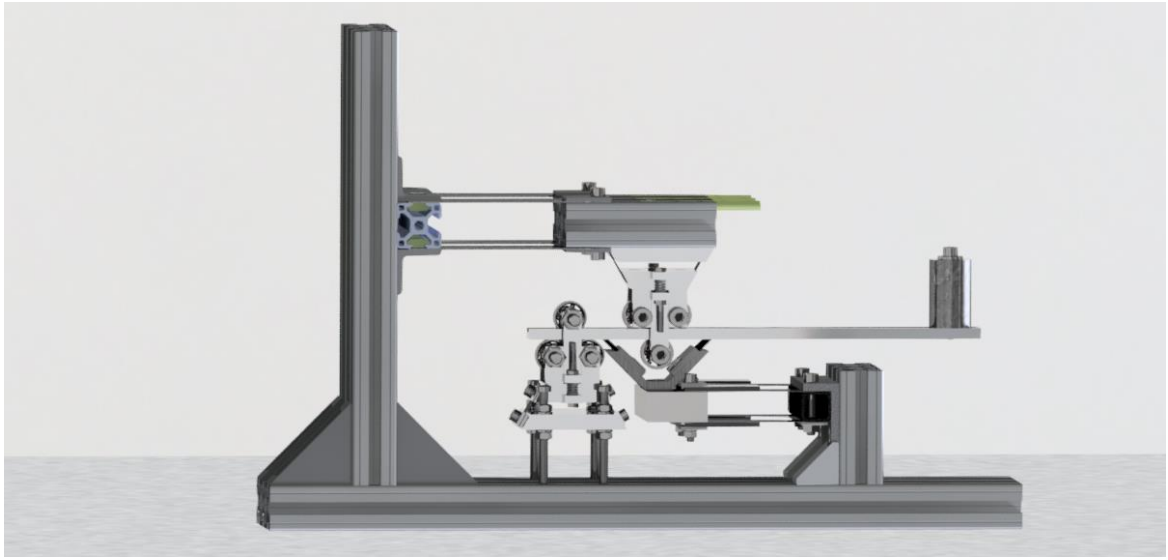


Figure 4.2. The 3D model of the experimental set-up

The following features replace the components of the idealized system in the prototype system:

- The sensing and actuation are carried out with rubber pads connected to a mass block softly suspended with leaf springs. Sheets of rubber are sticked to half of the length of these springs for damping.
- The main spring is replaced with four leaf springs. These parallel springs constrain the motion of the mass, so that it can only vibrate vertically.
- Compliant hinges are designed to replace the revolute joints at the base and mass hinge of the idealized system.

- The lever is compressed between rollers in the compliant hinges. This replaces the telescopic joints enabling the adjustable lever ratio.

In order to show these features and explain the necessary design calculations, the system sub-assemblies and parts are described in detail below. Figure 4.3 shows the sub-assemblies of the whole system in different colors. Here, the base and its hinge are in copper, the payload, its hinge and supporting leaf springs are in yellow, the actuator/sensor and the artificial ground mass are in blue and the lever is in gray.

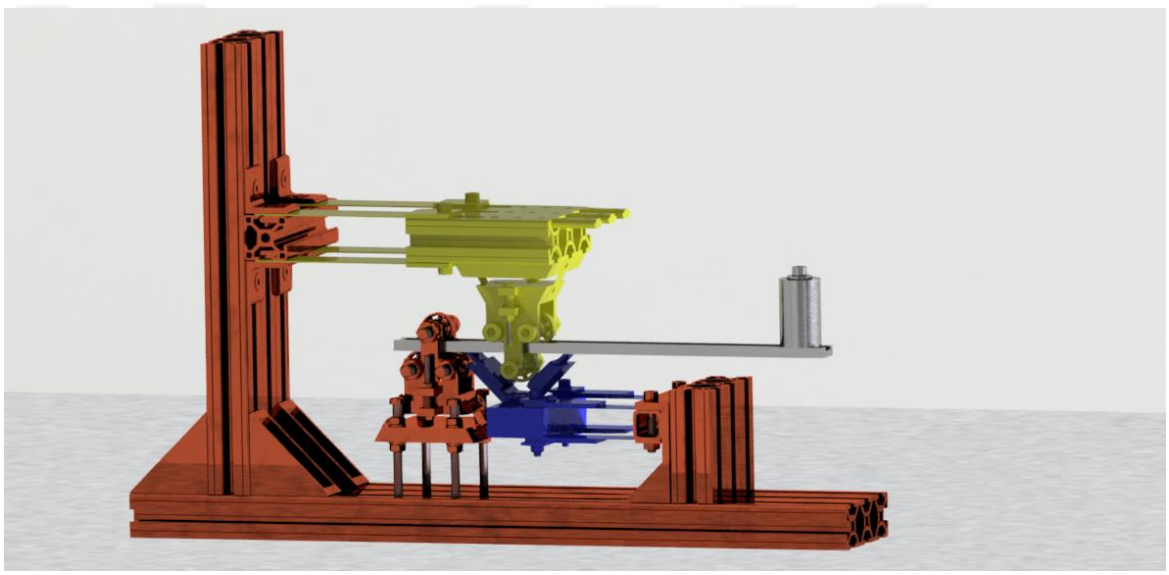


Figure 4.3. The overall system and its sub-assemblies shown in different colors

4.2.1. Sensor and Actuator Assembly

As described in the preceding chapters, the control algorithm requires the comparison of velocity at two locations on the lever and application of proportional forces for tuning. For this purpose, a vibro-impact type actuator, inserted on an inertia block is used. The vibro-impact actuator is a V-shaped block, in which rubber pads are compressed. The assembly is suspended with soft springs which are connected to base, for reduction of transient motion. The 3-D drawing of the assembly is shown in Figure 4.4 below.

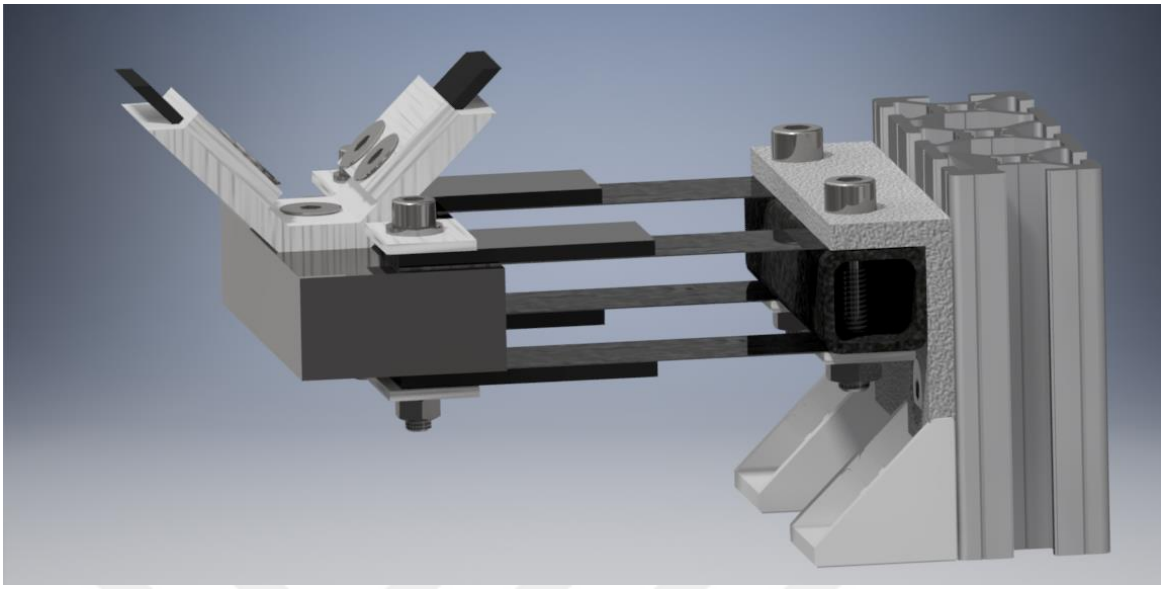


Figure 4.4. The sensor and actuator assembly shown as the V-shaped part with rubber pads on the artificial ground mass.

The V-shaped part in Figure 4.4 has two rubber pads pointing to opposite directions. As the lever vibrates, it impacts these pads, creating a normal force on each pad. Depending on the wedge angle, a tangential force is formed on each pad, as well. The impact actuator forces on the lever are shown in Figure 4.5 below.

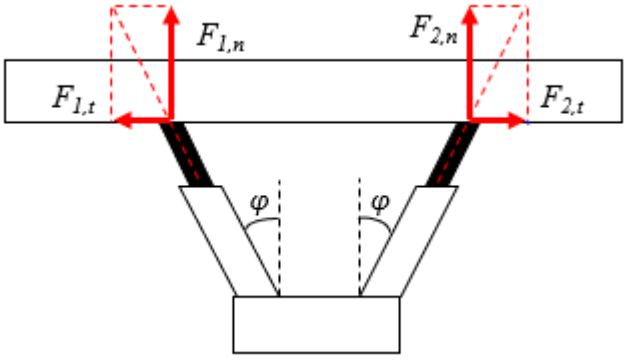


Figure 4.5 The actuator forces created by impact and the wedge angle

For a vibro-impact system with a wedge angle φ defined with respect to the vertical axis, the normal force (F_n) and tangential force (F_t) can be related in the absence of sliding as [64]:

$$tan\varphi = \frac{F_t}{F_n} \quad for\ tan\varphi < \mu_{friction} \tag{4.10}$$

For $tan\varphi > \mu_{friction}$, there is sliding in the system. For this case, the normal force and the tangential force can be related as follows:

$$\mu_{friction} = \frac{F_t}{F_n}, \qquad tan\varphi > \mu_{friction} \tag{4.11}$$

There are two rubber pads facing opposite directions, and they create two opposing tangential forces ($F_{1,t}$ and $F_{2,t}$ in Figure 4.5). The net tangential force created by these two pads ($F_{2,t}$-$F_{1,t}$) move the lever horizontally. As a result, the lever ratio changes. As mentioned in Chapter 3, the lever ratio changes until the antiresonance condition is achieved. At that point, the two horizontal forces are equal and the payload experiences minimum amount of vibration.

From Equation 4.10 and Equation 4.11, it is easy to see that $\mu_{friction}$ must be maximized in order to increase efficiency in moving the lever horizontally. Moreover, because the impacts cause non-linear responses in systems, the presence of damping in the actuator is also beneficial. Considering these two factors, rubber pads are utilized at the impacting points. The friction coefficient between the rubber pads and the aluminum lever is found to be approximately 0.5. Hence, if the wedge angle is less than 26°, then Equation 4.10 can be used. Various wedge angles are considered during the tests. When the wedge angle is less than 30°, excessive bouncing happens, and the horizontal lever motion is not effective. If the wedge angle is larger than 45°, then the rubber pads deform transversely, and they do not transmit much horizontal force. Around 45° wedge angle, a considerable amount of horizontal force is generated that can move the lever without experiencing bouncing. Hence, the wedge angle is fixed to 45° for all the subsequent tests.

The forces applied by the actuator are proportional to the impact velocity at these two locations. However, the impact force must be proportional to the velocity of these positions

in the inertial reference frame. If the actuator is connected to the base or the mass or any other component of the system, then the force will be proportional to the relative velocity between the impact location on the lever and this component. In order to overcome this problem, a means to keep the actuator stationary in the inertial reference frame is necessary. This is achieved with a softly suspended inertia block. The high mass of the inertia block enables it to act as an artificial ground, minimizing the motion due to impacts. This block is designed as a single piece as shown in Figure 4.4. However, its mass is increased in experiments to decrease its mobility. In order to neutralize its motion due to impacts, it is fixed to the base with soft leaf springs. Moreover, rubber sheets are glued on these, through half of their total length as shown in Figure 4.4. Application of rubber layer to only half of the spring enables facilitation of damping without increasing the spring constant significantly. Another important measure is the prevention of its rotation. If the block rotates about the out of plane axis, the height of the tips of the rubber pads will not be equal so the forces applied to the right and left parts will not be able to compare the velocity of two locations correctly. Therefore, four leaf springs are used in the system, forming a compliant analogue of the parallel mechanism. The parallel mechanism enables movement in the plane without a change in the orientation. The finite element simulation of the parallelogram mechanism of inertia mass is shown in Figure 4.6. The figure shows the horizontal (x-displacement) component and it can be seen that the x-displacement is nearly zero for the inertia block while its y-displacement is on the order of centimeters. Therefore, the system stays level in the horizontal axis.

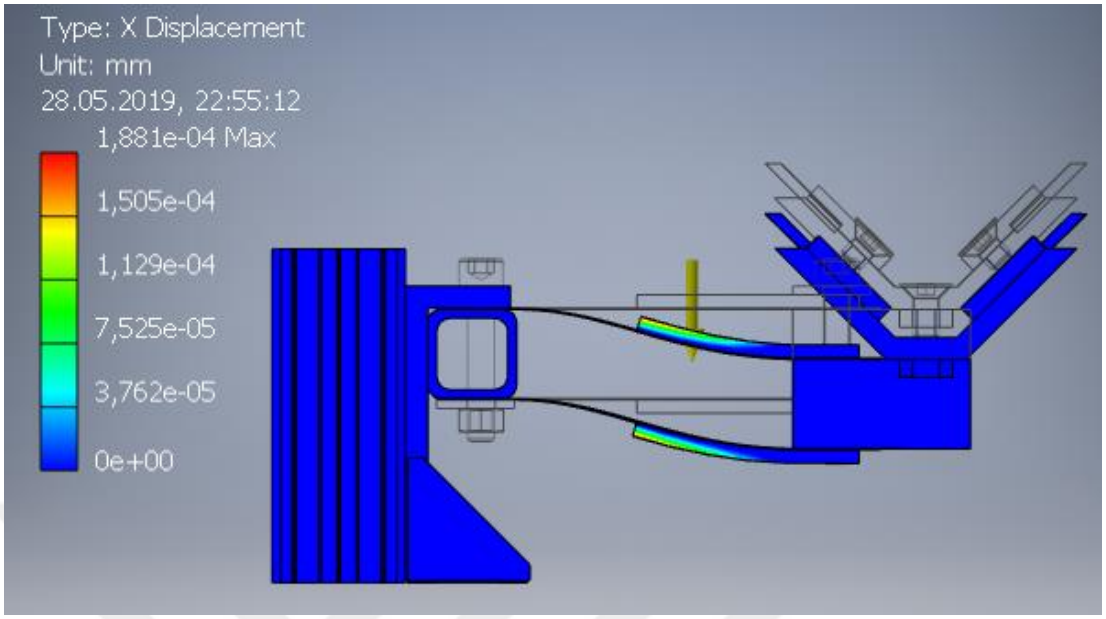


Figure 4.6. Linear finite element analysis regarding the parallel motion of the inertia block assembly

Even though the inertia block is connected to the base to prevent its motion, the base is not stationary in the inertial frame. Therefore, the effects of base motion on the inertia block must be minimized. This is achieved by keeping the springs soft so that the natural frequency of the sub-assembly is lower than system operating frequencies, providing vibration isolation. Meirovitch gives the stiffness coefficient for an Euler-beam which has a mass attached to its tip by the following formula [66]:

$$k = \frac{12EI}{L^3} \tag{4.12}$$

This formula is valid for systems in which the mass of the spring is negligible compared to other parts of the system.

Table 4.1 tabulates the parameters of the inertial-ground and shows the natural frequency calculations with the given parameters according to (4.12):

Table 4.1. Artificial ground system parameters

Spring Length (L)	130	mm	Young modulus (E)	206	GPa
Spring width (w)	16.5	mm	Spring constant ($k_{cantilever}$)	0.8	N/mm
Spring height (h)	0.5	mm	Mass (m_{ground})	1102	gr
Moment of inertia (I_{xx})	0.17	mm^4	Natural frequency (ω_p)	4.2	Hz

The operating frequency of the prototype starts with 20 Hz. With the designed natural frequency of the inertia block and neglecting damping, the transmissibility is less than 5%. As a result, it acts like an artificial ground, which is almost stationary as all the other parts of the system are vibrating.

4.2.2. The Payload Sub-Assembly

The payload sub-assembly consists of the payload, the main springs and the payload (mass) hinge. The 3-D drawing of this system is shown in Figure 4.7 below.

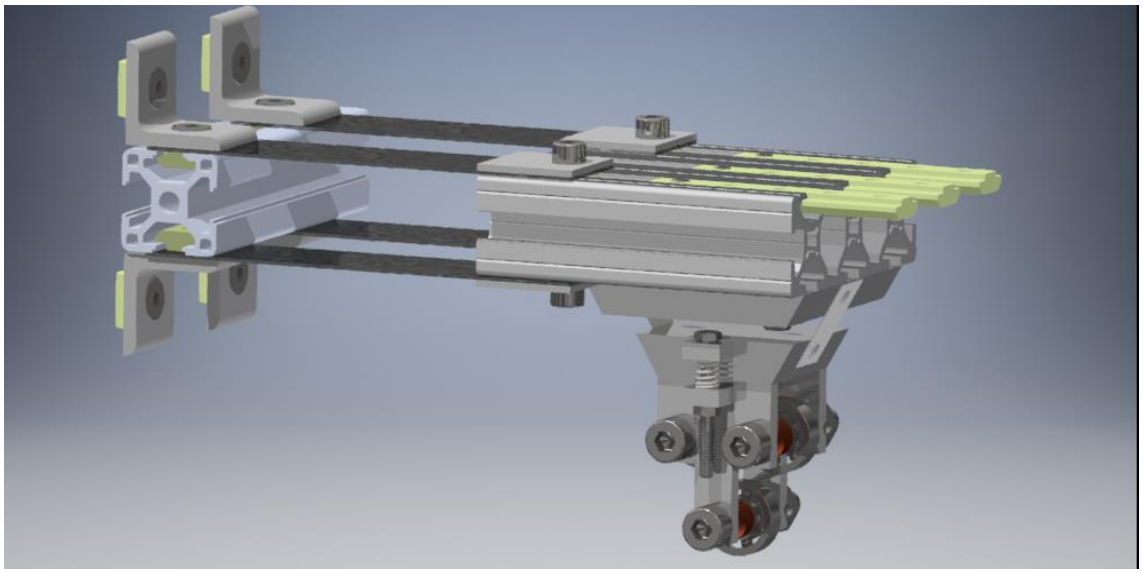


Figure 4.7. The payload sub-assembly

Four leaf springs are used in this sub-assembly as in the artificial ground system, benefiting from the parallel mechanism. The stiffness coefficient of payload springs is found with Equation 4.12. Note that the hinge above the lever adds to the payload mass in the frequency calculations. The payload parameters and the natural frequency calculations without lever effects (ω_0) are given in Table 4.2. The designated mass is the total mass of payload and hinge.

Table 4.2. Parameters and natural frequency calculations for payload

Spring length (L)	85	mm	Young modulus (E)	206	GPa
Spring width (w)	30	mm	Spring constant ($k_{cantilever}$)	40	N/mm
Spring height (h)	1.0	mm	Mass (M)	929	gr
Moment of inertia (I_{xx})	2.50	mm^4	Frequency (ω_0) (without isolator)	33.1	Hz

The idealized system described in previous chapters includes hinges for the inertial amplification mechanism. However, real hinges are multi-body devices which depend on gaps between elements to enable the rotational DOF with minimum friction, while hindering translational motion. For vibrational systems where amplitudes of motion are very small, these gaps act as drains which would swallow the low amplitude motion. This would prevent consistent operation of the system and repeatability of the measurements. Therefore, compliant hinges are designed in place of revolute hinges.

The compliant hinges benefit from two soft leaf springs to enable rotation about a point. The location of this point is at the extension of these springs as shown in Figure 4.8.

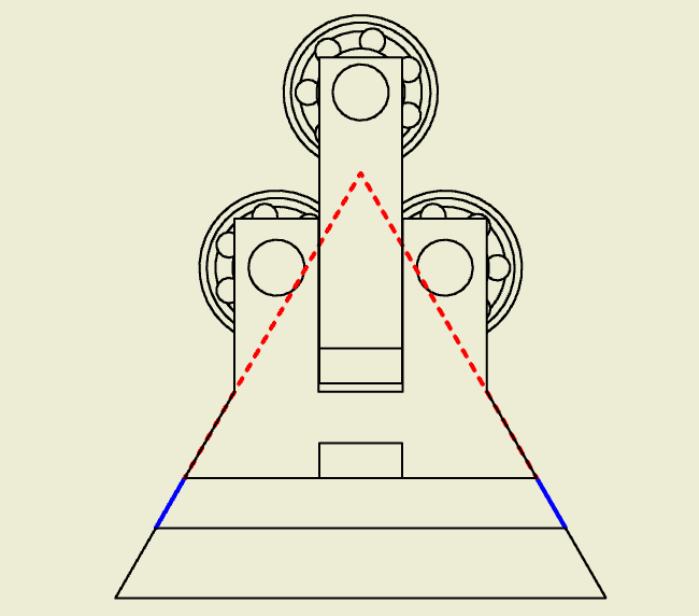


Figure 4.8. The leaf springs (in blue) and their extensions (in red) forming rotation center

The system includes three roller bearings which can be compressed by means of a compression bracket and two helical springs. When compressed, these bearings prevent backlash or gaps in the system while minimizing friction for horizontal lever movement. This mechanism also gives control over the amount of friction in the system. By changing the normal force on the bearings, the horizontal friction coefficient can be adjusted. The exploded view of the hinge is given in Figure 4.9.

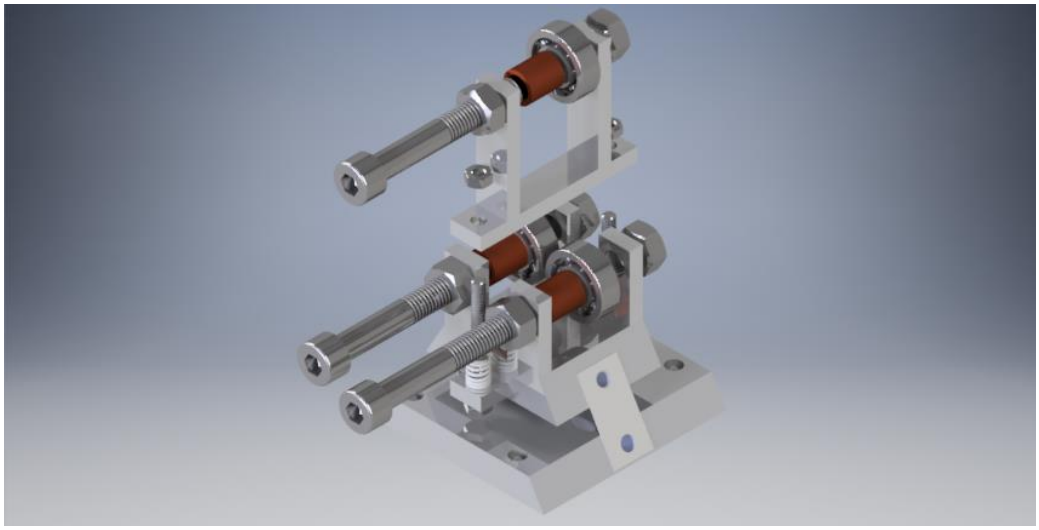


Figure 4.9. The exploded view of the hinge

The stiffnesses of the flexure hinges are part of system stiffness and must be included in FRF calculations. However, their calculation is different from the stiffness coefficient calculations of the parallel mechanism. This is because the end load condition contains both a force and a moment. The operation of the compliant hinge is analogous to a planar four-bar mechanism. The deformed geometry of the mechanism obtained by finite element analysis is shown in Figure 4.10.

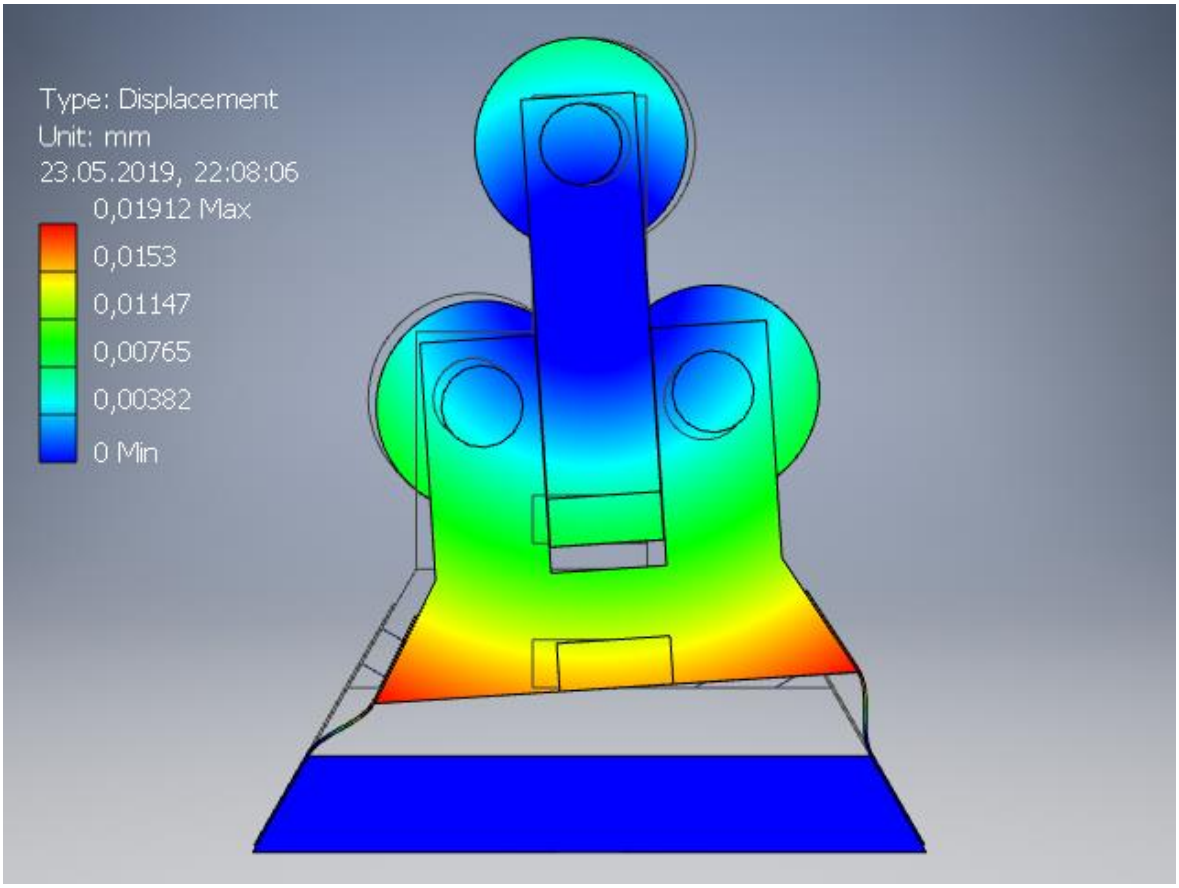


Figure 4.10. The deformed geometry of hinges obtained by linear finite element analysis

Howell *et al.* [67] suggest the application of pseudo-rigid-body models for the analyses of such mechanisms. The spring constant can be calculated by considering a four-bar linkage. Figure 4.11 shows the parameters of a four-bar linkage, which are used in the stiffness calculations.

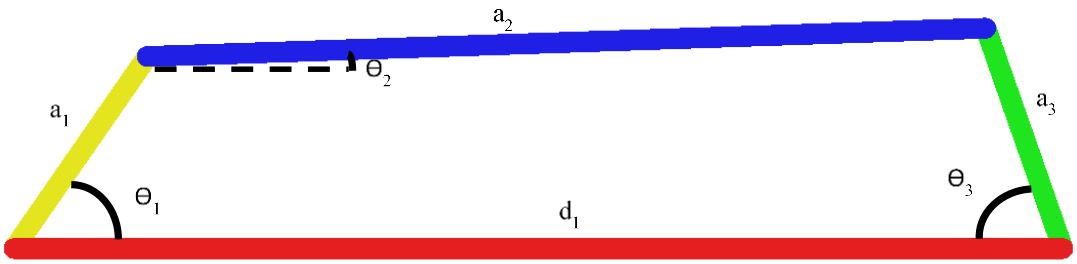


Figure 4.11. Parameters for hinge calculations

Writing the loop equation for y-direction:

$$a_1 sin\theta_1 + a_2 sin\theta_2 = a_3 \sin\theta_3 \tag{4.13}$$

For small angles $\theta_2 \ll 1$, $a_2 sin(\theta_2) \approx \theta_2$ and $a_1 = a_3$

$$\theta_2 = \frac{a_1}{a_2}(\sin\theta_3 - sin\theta_1) \tag{4.14}$$

At the initial position, both $\theta_1$and θ_3 are 60° or π/3 rad. Therefore θ_1 and θ_3 can be written in the following form:

$$\theta_1 = \frac{\pi}{3} + \theta'_1\,, \qquad \theta_3 = \frac{\pi}{3} + \theta'_3 \tag{4.15}$$

Where θ'_1 and θ'_3 are the changes in the magnitude of θ_1 and θ_3. Applying well-known trigonometric summation formula:

$$\theta_2 = \frac{a_1}{a_2} 2sin\left(\frac{\theta_3 - \theta_1}{2}\right) \cos(\frac{\theta_3 + \theta_1}{2})$$
$$\Rightarrow \theta_2 = \frac{a_1}{a_2} 2sin\left(\frac{\theta'_3 - \theta'_1}{2}\right) \cos(\frac{2\pi}{3} + \theta'_3 + \theta'_1) \quad (4.16)$$

During the operation of the mechanism, θ'_1 and θ'_3 always have opposite signs. Moreover, for small amplitudes of motion $|\theta'_1| \ll 1$ & $|\theta'_3| \ll 1 \Rightarrow |\theta'_3 + \theta'_1| < |\theta'_3 - \theta'_1| \ll 1$. Therefore,

$$\cos\left(\frac{2\pi}{3} + \theta'_3 + \theta'_1\right) \approx \cos\left(\frac{2\pi}{3}\right) = 0.5\,, \qquad sin\left(\frac{\theta'_3 - \theta'_1}{2}\right) \approx \frac{\theta'_3 - \theta'_1}{2} \quad (4.17)$$

Hence,

$$\theta_2 = \frac{a_1}{a_2}\left(\frac{\theta'_3 - \theta'_1}{2}\right) \Rightarrow |\theta_2| = \frac{a_1}{a_2}\left(\frac{|\theta'_3| + |\theta'_1|}{2}\right) \quad (4.18)$$

The spring constant for a cantilever with a moment and vertical force at the tip are $\frac{EI}{L}$ and $\frac{3EI}{L^3}$ respectively. If the free end is clamped to a mass, hindering the angular deflection and changing the boundary conditions, the spring constant can be approximated to be $\frac{12\mathrm{EI}}{\mathrm{L}^3}$. For this problem, both moment and force are applied at the tip and the tip is constrained to a rigid part, therefore none of the above can be applied directly. For this condition, Su *et al* [68] gives an approximate formula by using pseudo-rigid body model with four rigid bodies and three springs, which is validated for a four-bar link mechanism. Using this formula, the spring constant for each leaf-spring in the hinge can be obtained:

$$k_{link} \approx 0.99\frac{EI}{L} \quad (4.19)$$

For the flexure, the total deflection is the summation of the deflection of both hinges. In the deformed condition, as in Figure 4.10, both flexures move the hinge in the same direction. Therefore, both flexures contribute to the spring constant. The total spring constant can be found from the contribution of two:

$$k_{\theta,eq} \times \theta_2 = k_{\theta,eq} \times \frac{a_1}{a_2}\left(\frac{|\theta'_3| + |\theta'_1|}{2}\right) = k_{link}(|\theta'_3| + |\theta'_1|) \Rightarrow k_{\theta,eq} \approx 2EI\frac{a_2}{{a_1}^2} \quad (4.20)$$

The addition of the compliance of two hinges adds a second term to the potential energy term. However, with the small θ assumption, it can be combined in a single term:

$$V = \frac{1}{2}k(y_2 - y_1)^2 + 2 \times \frac{1}{2}k_{\theta,eq}\theta^2 \Rightarrow V = \frac{1}{2}(k + 2\frac{k_{\theta,eq}}{{l_2}^2})(y_2 - y_1)^2 \quad (4.21)$$

Therefore, the total system stiffness becomes:

$$k_{eq} = k + 2\frac{k_{\theta,eq}}{{l_2}^2} \quad (4.22)$$

The hinge parameters and stiffness calculations are summarized in Table 4.3.

Table 4.3. The hinge parameters and stiffness calculations

a_1	8.2	mm	Moment of inertia (I_{xx})	0.02	mm^4
a_2	50.2	mm	Young modulus (E)	206	GPa
Height (h)	15.0	mm	k_{link}	483	Nmm/rad
Width (w)	0.3	mm	$k_{\Theta,eq}$	5896	Nmm/rad

4.2.3. The Base Sub-Assembly

The frame of the system is constructed from aluminum sigma profile blocks, as shown in Figure 4.12. Sigma profiles enable flexibility in system design and do not reduce transmissibility. The system contains leaf springs and other flexible elements whose deflected position cannot be calculated exactly. However, the sigma profile system enables re-locating system components on necessity.

As shown in Figure 4.12, this assembly contains a hinge as well. It is connected to the frame with four M6 studs and compression brackets. This type of assembly enables re-locating the hinge in both vertical and horizontal directions. Re-location in horizontal direction enables changing l_2 during experiments. DOF in vertical enables altering the system alignment and pre-compression, which are important in tuning and operation.

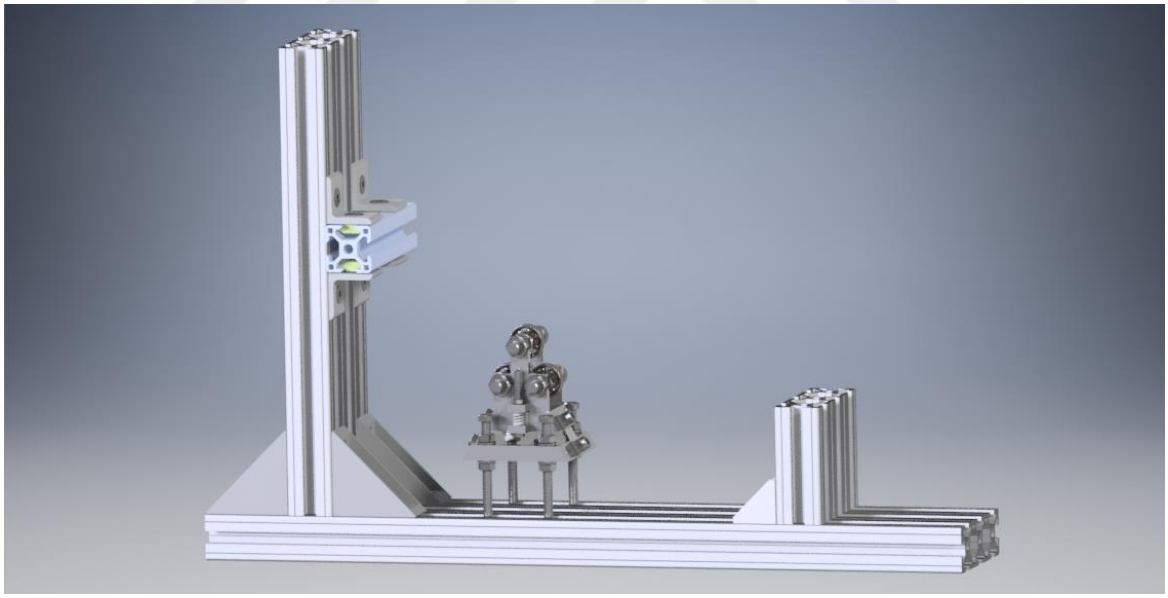


Figure 4.12. The system frame and base

4.2.4. The Isolator Sub-Assembly

The cylindrical (point) mass and the lever, together with the hinges constitute the isolator. For the continuous isolator, the positioning of the center of gravity and the rotational

inertia of the isolator affect the FRF. System data and calculations results are tabulated in Table 4.4.

Table 4.4. Gravitational center and mass moment of inertia calculations for the isolator

Length (l_{tot})	300	mm	Isolator mass location (l_{is})	280	mm
Lever mass (m_l)	127	gr	Center of gravity (l_3+u)	227	mm
Isolator mass (m_{is})	182	gr	I_z (total, wrt mass center)	$2.2x10^6$	gr-mm^2

4.3. Total System Response and the Critical Frequencies

The parameters can be plugged in Equation 4.8 and Equation 4.9 to calculate the critical frequencies for the distributed parameter system. The pole and zero frequency calculations for the set-up at three different lever positions are given in Table 4.5:

Table 4.5. Pole and zero frequencies for three different lever positions

	Lever position			
	100 mm	**130 mm**	**190 mm**	**Unit**
ω_p	21.8	19.5	15.4	Hz
ω_z	34.0	28.3	19.9	Hz

The position of the lever and the configuration of the set-up for these three cases is shown in Figure 4.13 below.

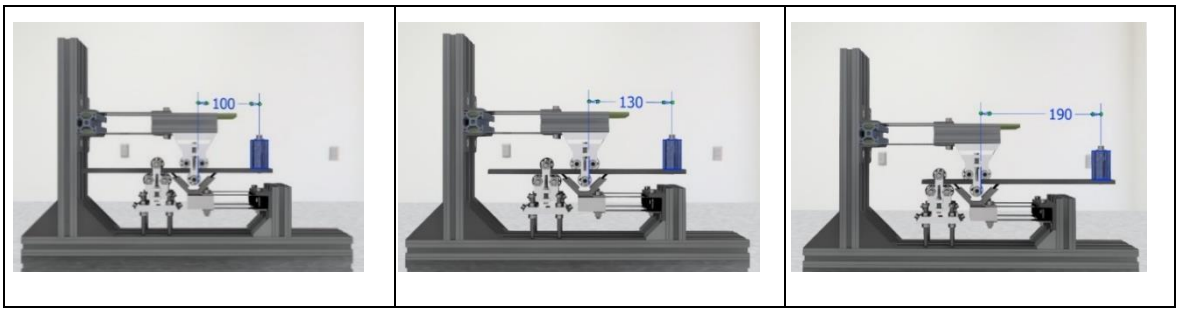


Figure 4.13. The lever in leftmost (100 mm position), middle (130mm) and rightmost (190mm) positions

Notice that from Table 4.5, it is seen that the antiresonance frequency varies between 20 and 34 Hz for these system configurations. Hence, vibration isolation is possible within this frequency range by adjusting the antiresonance frequency to the excitation frequency. The frequency range of operation can be improved by decreasing l_2 in the system or increasing the lever length. However, in order to fit the inertia block, the actuator pads and the hinges, the distance between hinges is kept at 55 mm. Moreover, the length of the lever is chosen as 300 mm.

5. EXPERIMENTAL RESULTS

After the system assembly, it is connected to an LDS V450 shaker and DSC4 sine controller for vibration testing. Two 3273A2 Model Dytran accelerometers are used in the system, one for the base and one for the payload mass. The data is collected with a two-channel Polytec data acquisition device. Moreover, one Brüel&Kjaer Type 4382 accelerometer is installed on the base and connected directly to the controller of the shaker for closed loop operation. The system is shown in Figure 5.1 connected to the shaker.



Figure 5.1. The experimental set-up without the sensor and data logger

In the first set of experiments, the FRF for the lever–spring and mass system is measured without the action of the artificial ground mass. The connection of the rubber actuators with the lever is cut and sine sweep test is carried out at the three different positions of the lever, shown in Figure 4.13 to compare the analytical pole and zero frequency calculations in Table 4.5 with the experimental results.

The data obtained from these sine-sweep tests has noise. In order to improve them, a ten – element moving average filter is applied. The resulting FRF graphs for the three cases are given in Figure 5.2 below. According to these measurements, the resonance (pole) and antiresonance (zero) frequencies are obtained. The experimental results for these frequencies are tabulated together with calculated values obtained in Chapter 4 in Table 5.1 below.

Table 5.1. Pole and zero frequencies for three different lever positions

	Calculated			Experimental			
	Lever Position (mm)			Lever Position (mm)			
Frequency	100	130	190	100	130	190	Unit
ω_p	21.8	19.5	15.4	21.4	19	15.6	Hz
ω_z	34	28.3	19.9	33.4	28.1	20.3	Hz

It is seen from Table 5.1 that the experimental and analytical values are in close agreement, with less than 3% error for all cases mentioned.

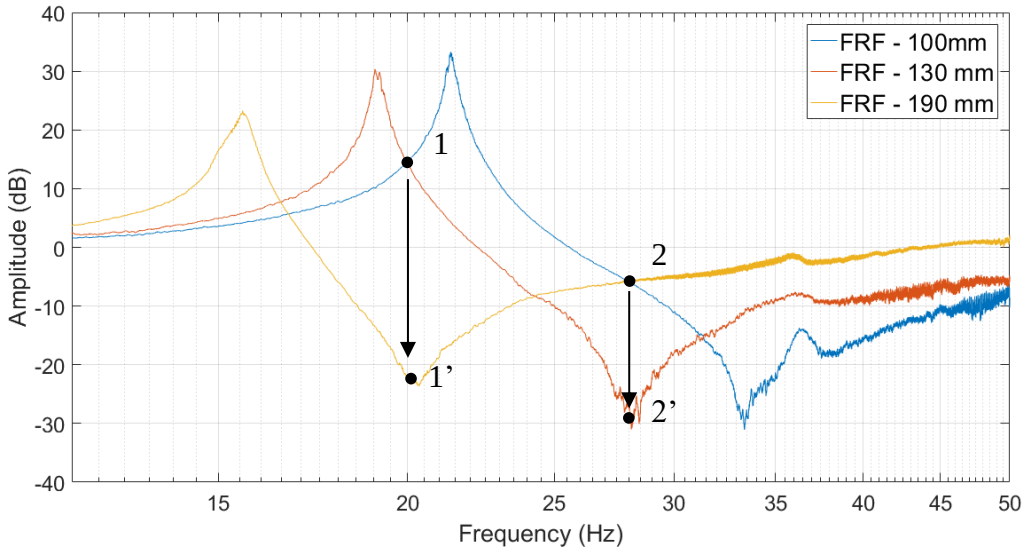


Figure 5.2. FRF for three different lever positions

The FRF plots show that the zero frequency ω_z shifts from 20 Hz to 33 Hz with lever position change from the rightmost to the leftmost position. However, at the leftmost

position, the lever collides with the vertical block of the base and this creates unrelated harmonics in the measurements. Therefore, the test range is limited between 20 Hz to 30 Hz.

An important parameter to be tuned is the initial normal force between the rubber pads of the artificial ground mass and the isolator. Various normal forces from 0.2 N to 5 N are tested. At high normal forces, the tuning speed increases but the additional damping added to the system diminishes the antiresonance effect. At very low normal force values the horizontal force is not enough to overcome the friction in the bearings. After many tests, the optimum value is determined to be 0.7 N. The system is tuned to this normal force value for all the subsequent measurements.

The first experiment is with 20 Hz constant frequency excitation while the lever is at the left-most position (100 mm in Figure 4.13). At the initial condition, the system's antiresonance frequency is at 33Hz (see Table 5.1). This configuration of the system corresponds to point 1 in Figure 5.2. For the system to tune itself to 20 Hz, it must reach point 1' shown again in Figure 5.2. However, as the lever moves right, the system natural frequency decreases, i.e., ω_n is lower for the red and yellow curves. Therefore, the output is expected to pass through a resonance first, and then decrease. This behaviour is similar to the behaviour observed in MBD simulations for Case 1 in Chapter 3. Please refer to Figure 3.3 for the related simulation results. Experimental results agree with the expected behaviour, as seen in Figure 5.3. Notice that the red lines are transparent and darker parts show obscured data, namely the input.

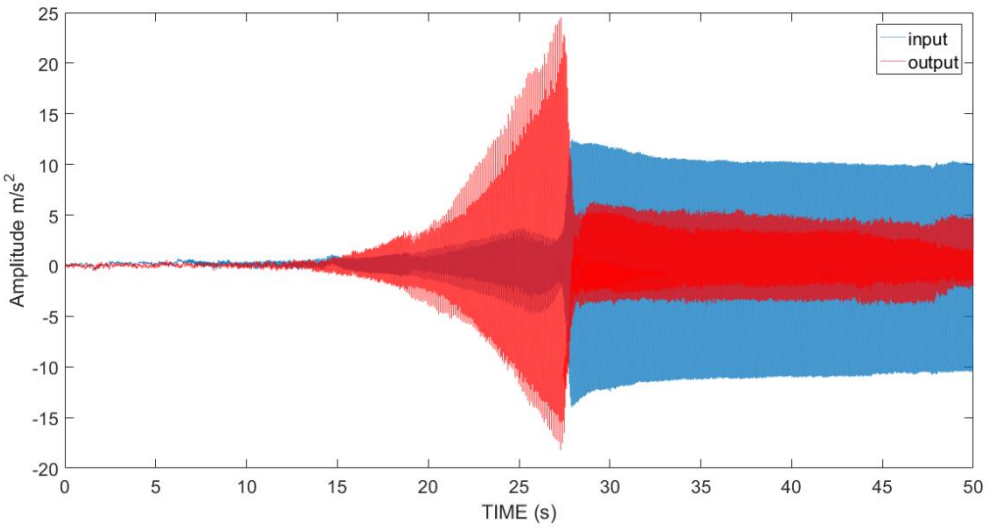


Figure 5.3. Self-tuning of the system to 20 Hz input excitation

The next experiment is the application of 30 Hz input while the lever is at the right-most position (190 mm in Figure 4.13). At this initial condition, the system's antiresonance frequency is at 20 Hz (see Table 5.1). This is similar to moving from point 2 to 2' in Figure 5.2 at 28 Hz excitation. For the numerical simulations in Chapter 3, it corresponds to Case 5 shown in Figure 3.7. The expected behaviour is starting with low output and decrease further. As shown in Figure 5.4, the results are again in agreement with this behaviour.

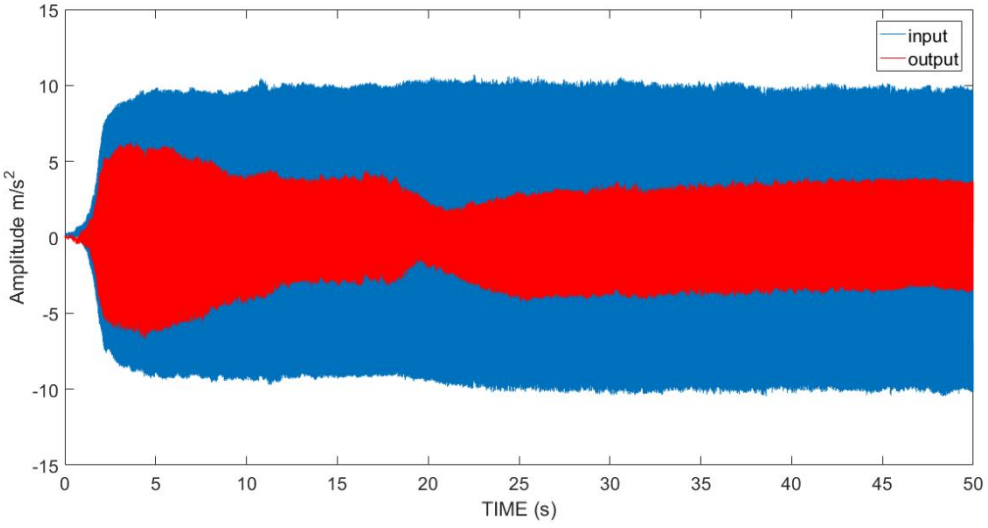


Figure 5.4. Self-tuning of the system to 30 Hz excitation

After constant frequency experiments, sweep tests were conducted. Starting from ω_z of a certain configuration, a sine-sweep input is applied. The output is expected to follow the excitation and always keep the system in isolation (output remains less than the input). Figure 5.5 shows the system start from 30 Hz and fall to 20 Hz with a rate of 10 Hz/min. Figure 5.6 shows the system start from 20 Hz and go up to 30 Hz with a rate of 10 Hz/min. Notice that in both cases, the output amplitude is always lower than the input amplitude showing that the system self-tunes to the changing excitation frequency. FRF graphs for these experiments are shown in Figure 5.7 and Figure 5.8. The sweep tests are carried out in 20-30 Hz frequency band and both curves achieve low amplitude values in this range.

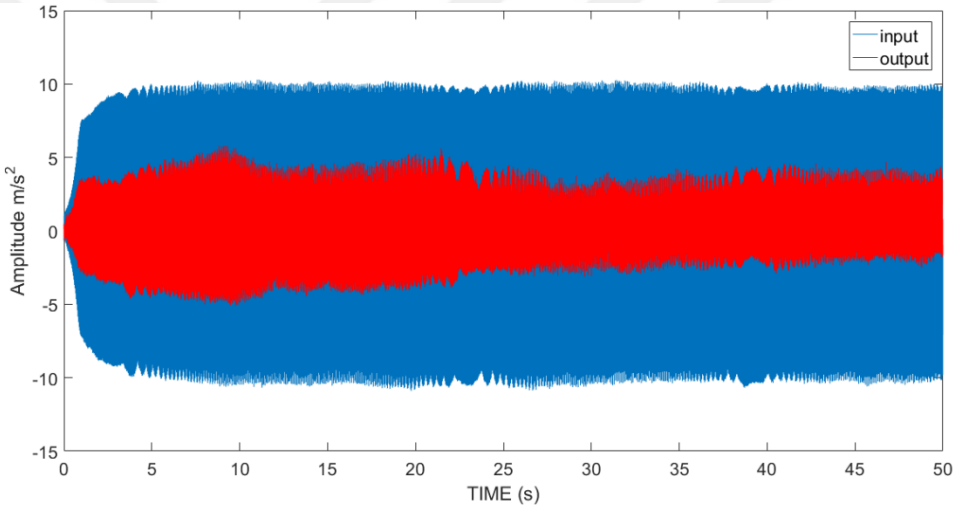


Figure 5.5. Response of the system during a frequency sweep from 30 Hz to 20 Hz at 10 Hz/min

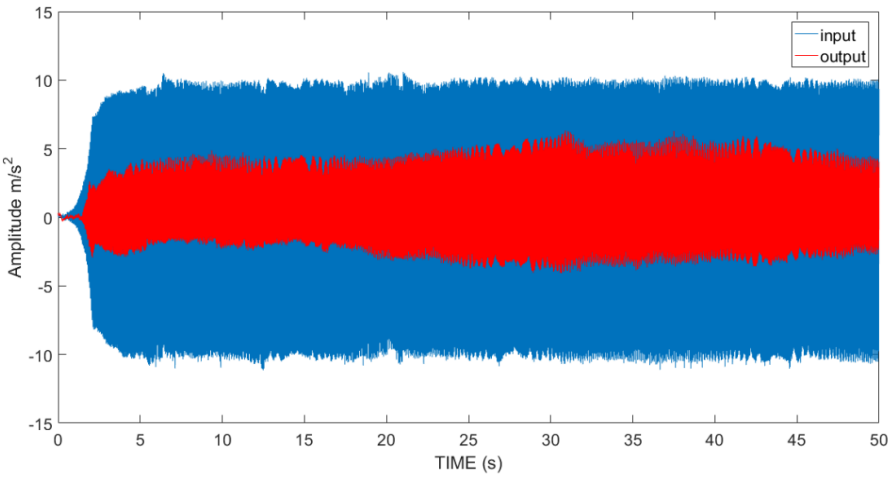


Figure 5.6. Response of the system during a frequency sweep from 20 Hz to 30 Hz at 10 Hz/min

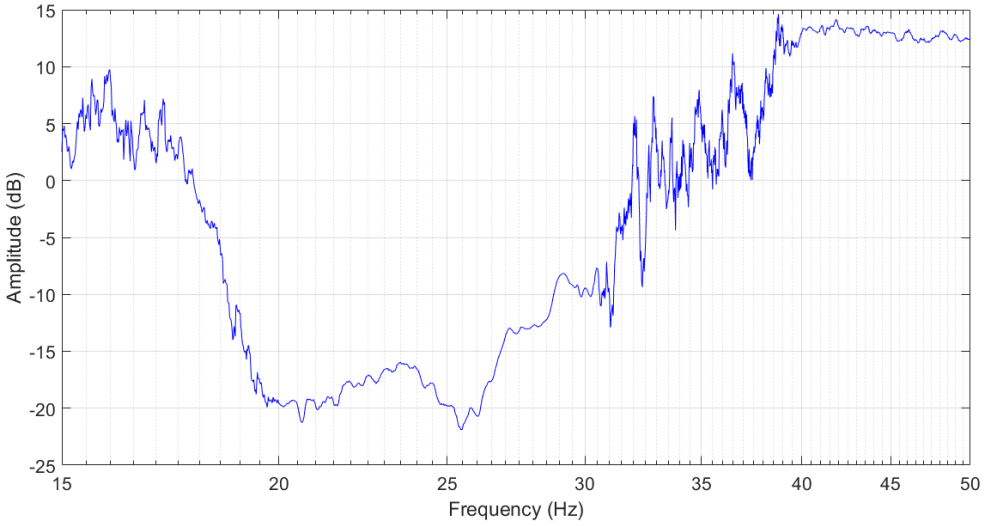


Figure 5.7. FRF of frequency sweep from 30 Hz to 20Hz

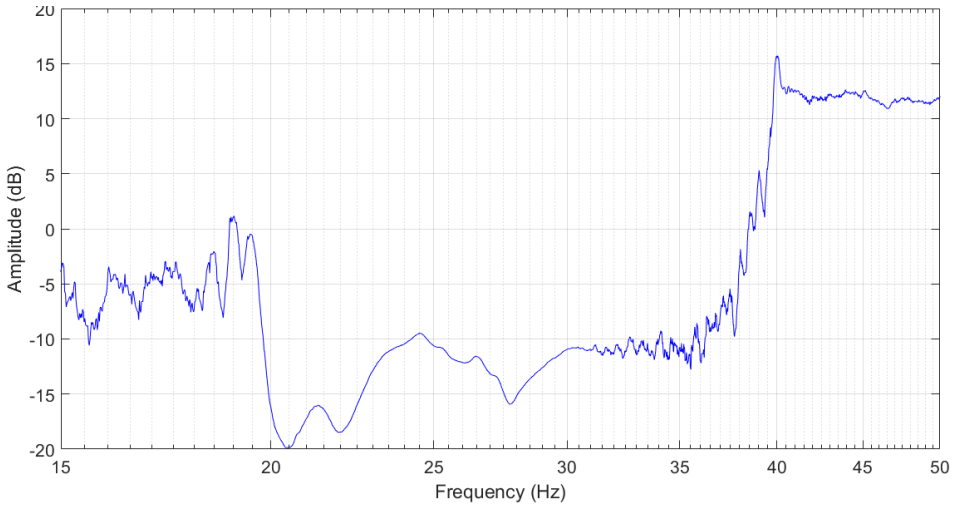


Figure 5.8. FRF of frequency sweep from 20 Hz to 30 Hz

The final test is visualization of the instant center location on the actual system. For this purpose, the set-up is left to tune itself at a constant frequency. After tuning is completed, a photograph of the set-up is taken with long exposure. The photograph in Figure 5.9 shows that the system is able to tune the instantaneous center of zero velocity to the mass hinge location where the image is very sharp. Other parts of the system are blurry because of the vibrations. Notice that the artificial ground mass is also very sharp proving that it remains stationary as the base moves.

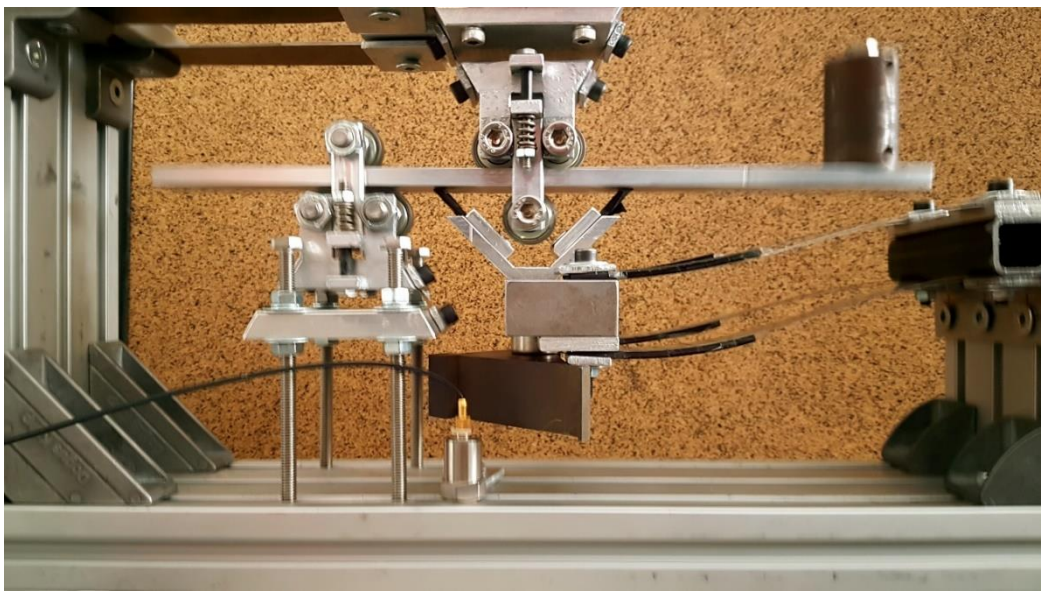


Figure 5.9. Long exposure photograph of the set-up under constant frequency excitation

6. CONCLUSION

6.1. Summary

In this thesis, a control algorithm for a passive self-tuning lever-type vibration isolator is developed. An experimental system employing this algorithm is designed and tested.

The performance of passive vibration isolation systems may not meet the performance requirements due to changing operating conditions. However, the designed self-tuning mechanical system can respond to these changes by altering its parameters.

The control algorithm is developed from the lumped parameter analysis of the system. The MBD simulations with lumped parameters show that the algorithm works for all frequency ranges. After the lumped analysis, a distributed parameter model of the system is created. For the distributed parameter case, the control rule still applies but the frequency range is less than the lumped parameter case. This is due to the limits on the lever ratios achievable with a distributed parameter system.

An experimental variable lever ratio isolator assembly is constructed with compliant hinges. The distributed parameter model of the system is used in the derivation of critical frequencies of this experimental set-up. Sine-sweep test results are in agreement with the values obtained from the analytical model. Consequently, the control scheme is applied to the test bench through the use of an artificial ground mass and a vibro- impact type actuator. The set-up is base excited with various fixed frequencies that are below and above the resonance and antiresonance frequencies of the system and its response is monitored in each case. The experimental results show that the system always tunes itself to the excitation frequency to minimize vibration transmission. Following the constant frequency tests, sine sweep tests are applied. The system tunes itself in response to the changes in the excitation frequency and adapts the lever ratio accordingly. Finally, a long exposure photo of the set-up is taken after the system self-tuned to a constant excitation. The blurriness of a location in such a photo is an indicator of the amount of motion experienced. The results point out

that the instant center of zero velocity of the lever coincides with the payload hinge location, as expected. Moreover, the softly suspended artificial ground mass appears stationary, validating it as a reference to the inertial frame.

6.2. Future Work

This study is aimed at filling the gap in the knowledge of adaptive, mechanically tuned passive vibration isolators. The study concentrates on the creation and validation of the control algorithm. The system is assumed to be linear and the detrimental effects of non-linearities on the performance are not diagnosed and improved. The damping caused by the non-symmetrical impact conditions and the corresponding back and forth motion of the lever in a vibration cycle, friction, gravitational deflection and vibro-impact effects are the evident sources of non-linearities that can be inspected in future studies.

The current system has been designed for single – frequency vibration excitations. It can track the excitation and tune itself even if this single excitation frequency changes. However, if multiple frequencies are applied simultaneously, the system design must be modified accordingly.

The working frequency range of this set-up is limited by the geometry of the isolator and geometrical constraints. However, even if these are improved, there is a limit to the working frequency range due to the limitations of the vibro-impact type actuator. As the working frequencies increase, the vibration amplitudes decrease. As the current rubber pads have low transverse stiffness, they cannot move the lever at small amplitude motion. For high frequency applications shorter and stiffer rubber pads can be used. This will increase the forces created by the actuator even under low amplitude of motion.

The system setting time is dependent on the compressive preload on the rubber pads, the excitation frequency and amplitude. For higher excitation frequencies and amplitudes, the settling time is smaller. Moreover, as the preload increases, the transverse forces increase, as well. Consequently, the system tuning time drops. However, constant contact

with the rubber pads increases system damping. Optimization of these two variables can be the subject of future studies.

REFERENCES

1. Brandt, A., *Noise and Vibration Analysis: Signal Analysis and Experimental Procedures*, Wiley & Sons, Chichester, West Sussex, U.K. ; Hoboken, N.J., 2011.

2. Thorby, D., *Structural Dynamics and Vibration in Practice : An Engineering Handbook*, Elsevier/Butterworth-Heinemann, Amsterdam, Boston, London, 2008.

3. Silva, C.W. de, *Vibration and Shock Handbook*, Taylor & Francis Group, Boca Raton, 2005.

4. Piersol, A.G., T.L. Paez, *Harris' Shock and Vibration Handbook*, 6th Ed., McGraw-Hill, New York, 2010.

5. Jones, R., J.H. McGarvey, "Helicopter Rotor Isolation Evaluation Utilizing the Dynamic Antiresonant Vibration Isolator", *SAE Technical Paper 760894*, 1976.

6. Flannely, W.G., "Dynamic Antiresonant Vibration Isolator", US Patent no 3322379, 1970.

7. Braun, D., "Development of Antiresonance Force Isolators for Helicopter Vibration Reduction", *Journal of the American Helicopter Society*, Vol. 27, pp 37–44, 1982.

8. Yilmaz, C., N. Kikuchi, "Analysis and Design of Passive Band-Stop Filter-Type Vibration Isolators for Low-Frequency Applications", *Journal of Sound and Vibration*, Vol. 291, pp 1004–1028, 2006.

9. Yilmaz, C., *Analysis and Design of Uniaxial Passive Vibration Isolators Considering Stiffness and Bandwidth Limitations*, Ph.D. Dissertation, The University of Michigan, 2005.

10. Taylor, E.S., "Eliminating Crankshaft Torsional Vibration in the Radial Aircraft Engines", *SAE Technical Paper 360105*, 1936.

11. Horvath, R., G.T. Flowers, J. Fausz, "Passive Balancing of Rotor Systems Using Pendulum Balancers", *Journal of Vibration and Acoustics*, Vol. 130, pp 041011 1-11, 2008.

12. Ishida, Y., "Recent Development of the Passive Vibration Control Method", *Mechanical Systems and Signal Processing*, Vol. 29, pp 2–18, 2012.

13. Nester, T.M., A.G. Haddow, S.W. Shaw, J.E. Brevick, V.J. Borowski, "Vibration Reduction in a Variable Displacement Engine Using Pendulum Absorbers", *SAE Technical Paper Series*, Vol. 1, 2010.

14. Narimani, A., M.E. Golnaraghi, G. Nakhaie Jazar, "Frequency Response of a Piecewise Linear Vibration Isolator", *Journal of Vibration and Control*, Vol. 10, pp 1775–1794, 2004.

15. Pranesh, M., R. Sinha, "VFPI : An Isolation Device for Aseismic Design", *Earthquake Engineering and Structural Dynamics*, Vol. 29, pp 603–627, 2000.

16. Koçak, K., *Design of a Compliant Lever-Type Passive Vibration Isolator Using Quasi-Zero Stiffness Mechanism*, M.S. Thesis, Boğaziçi University, 2011.

17. Sun, X., X. Jing, "Multi-Direction Vibration Isolation with Quasi-Zero Stiffness by Employing Geometrical Nonlinearity", *Mechanical Systems and Signal Processing*, Vol. 62–63, pp 149–163, 2015.

18. Sun, Y., J. Zhou, D. Gong, W. Sun, Z. Xia, "Vibration Control of High-Speed Trains Self-Excitation under-Chassis Equipment by HSLDS Vibration Isolators †", *Journal of Mechanical Science and Technology*, Vol. 33, pp 65–76, 2019.

19. Liu, C., X. Jing, Z. Chen, "Band Stop Vibration Suppression Using a Passive X-Shape Structured Lever-Type Isolation System", *Mechanical Systems and Signal Processing*, Vol. 68–69, pp 342–353, 2016.

20. Ibrahim, R.A., "Recent Advances in Nonlinear Passive Vibration Isolators", *Journal of Sound and Vibration*, Vol. 314, pp 371–452, 2008.

21. Foda, M.A., B.A. Albassam, "Vibration Confinement in a General Beam Structure During Harmonic Excitations", *Journal of Sound and Vibration*, Vol. 295, pp 491–517, 2006.

22. Fuller, C.R., A.H. von Flotow, "Active Control of Sound and Vibration", *IEEE Control Systems*, Vol. 15, pp 9–19, 1995.

23. Preumont, A., *Vibration Control of Active Structures , An Introduction*, 2.nd Ed., Kluwer Academic Publishers, Dordrecht, Boston, 2002.

24. Nakano, K., Y. Suda, S. Nakadai, "Self-Powered Active Vibration Control Using a Single Electric Actuator", *Journal of Sound and Vibration*, Vol. 260, pp 213–235, 2003.

25. Karnopp, D., "Active and Semi-Active Vibration Isolation", *Journal of Vibration and Acoustics*, Vol. 117, pp 177, 1995.

26. Karnopp, D., M.J. Crosby, R.A. Harwood, "Vibration Control Using Semi-Active Force Generators", *Journal of Engineering for Industry*, Vol. 96, pp 619–626, 1974.

27. Casciati, F., G. Magonette, F. Marazzi, *Technology of Semiactive Devices and Applications in Vibration Mitigation*, Wiley, Chichester, England ; Hoboken, NJ, 2006.

28. Liu, C., X. Jing, S. Daley, F. Li, "Recent Advances in Micro-Vibration Isolation", *Mechanical Systems and Signal Processing*, Vol. 56–57, pp 55–80, 2015.

29. Wang, B., L. Kari, "A Nonlinear Constitutive Model by Spring, Fractional Derivative and Modified Bounding Surface Model to Represent the Amplitude, Frequency and the Magnetic Dependency for Magneto-Sensitive Rubber", *Journal of Sound and Vibration*, Vol. 438, pp 344–352, 2019.

30. Hurlebaus, S., L. Gaul, "Smart Structure Dynamics", *Mechanical Systems and Signal Processing*, Vol. 20, pp 255–281, 2006.

31. Symans, M.D., M.C. Constantinou, "Semi-Active Control Systems for Seismic Protection of Structures: A State-of-the-Art Review", *Engineering Structures*, Vol. 21, pp 469–487, 1999.

32. Hong, S.R., S.B. Choi, Y.T. Choi, N.M. Wereley, "Non-Dimensional Analysis and Design of a Magnetorheological Damper", *Journal of Sound and Vibration*, Vol. 288, pp 847–863, 2005.

33. Domaneschi, M., "Semi-Active Electro-Inductive Devices : Characterization and Modelling", *Journal of Vibration and Control*, Vol. 13, pp 815–838, 2007.

34. Bajkowski, J.M., B. Dyniewicz, M. Gębik-Wrona, J. Bajkowski, C.I. Bajer, "Reduction of the Vibration Amplitudes of a Harmonically Excited Sandwich Beam with Controllable Core", *Mechanical Systems and Signal Processing*, Vol. 129, pp 54–69, 2019.

35. Azadi, M., S. Behzadipour, G. Faulkner, "Variable Stiffness Spring Using Tensegrity Prisms", *Journal of Mechanisms and Robotics*, Vol. 2, pp 041001, 2010.

36. Brennan, M.J., "Some Recent Developments in Adaptive Tuned Vibration Absorbers/Neutralisers", *Shock and Vibration*, Vol. 13, pp 531–543, 2006.

37. Acar, M.A., C. Yilmaz, "Design of an Adaptive–Passive Dynamic Vibration Absorber Composed of a String–Mass System Equipped with Negative Stiffness Tension Adjusting Mechanism", *Journal of Sound and Vibration*, Vol. 332, pp 231–245, 2013.

38. Christie, M.D., S. Sun, L. Deng, D.H. Ning, H. Du, S.W. Zhang, W.H. Li, "A Variable Resonance Magnetorheological-Fluid-Based Pendulum Tuned Mass Damper for Seismic Vibration Suppression", *Mechanical Systems and Signal Processing*, Vol. 116, pp 530–544, 2019.

39. Hollkamp, J.J., S. Ste, W.-P. Afb, T.F. Starchville, "A Self-Tuning Piezoelectric Vibration Absorber", *Journal of Intelligent Material Systems and Structures*, Vol. 5, pp 559–566, 1994.

40. Longbottom, C.J., M.J. Day, "Vibration Absorber", GB Patent no: 2189573, 1987.

41. Bailey, D.C., W. Jensen, A.H. von Flotow, C. Park, "Adaptively Tuned Elastomeric Vibration Absorber", European Patent no: 0922877, 1998.

42. Brzeski, P., T. Kapitaniak, P. Perlikowski, "Novel Type of Tuned Mass Damper with Inerter Which Enables Changes of Inertance", *Journal of Sound and Vibration*, Vol. 349, pp 56–66, 2015.

43. Brzeski, P., M. Lazarek, P. Perlikowski, "Experimental Study of the Novel Tuned Mass Damper with Inerter Which Enables Changes of Inertance", *Journal of Sound and Vibration*, Vol. 404, pp 47–57, 2017.

44. Duc La, V., C. Adam, "General On-off Damping Controller for Semi-Active Tuned Liquid Column Damper", *Journal of Vibration and Control*, Vol. 23, pp 5487–5501, 2018.

45. Viet, L.D., N.B. Nghi, N.N. Hieu, D.T. Hung, "On a Combination of Ground-Hook Controllers for Semi-Active Tuned Mass Dampers", *Journal of Mechanical Science and Technology*, Vol. 28, pp 2059–2064, 2014.

46. Hidaka, S., Y. Kong, A.S. Morishita, "Adaptive Vibration Control by a Variable-Damping Dynamic Absorber Using ER Fluid", *Journal of Vibration and Acoustics*, Vol. 121, pp 373–378, 1999.

47. Jalili, N., "A Comparative Study and Analysis of Semi-Active Vibration Control Systems", *Journal of Vibration and Acoustics*, Vol. 124, pp 593, 2002.

48. Dyke, S.J., B.F.S. Jr, "A Comparison of Semi-Active Control Strategies for the MR Damper", in: Adeli, P.H. (Ed.), *Proceedings Intelligent Information Systems*, Grand Bahama Island, Bahamas, 1997, IEEE, Los Alamitos, California, 1997.

49. Savaresi, S.M., C. Spelta, "Mixed Sky-Hook and ADD: Approaching the Filtering Limits of a Semi-Active Suspension", *Journal of Dynamic Systems, Measurement, and Control*, Vol. 129, pp 382, 2007.

50. Karnopp, D., "Force Generation in Semi-Active Suspensions Using Modulated Dissipative Elements", *Vehicle System Dynamics*, Vol. 16, pp 333–343, 1987.

51. Stanway, R., J.L. Sproston, A.K. El-Wahed, "Applications of Electro-Rheological

Fluids in Vibration Control: A Survey", *Smart Materials and Structures*, Vol. 5, pp 464–482, 1996.

52. Lloyd, W.B., "Variable Frequency Vibration Isolator", US Patent no: 4699257, 1987.

53. Alici, G., H. Du, W. Li, T. Tian, M. Nakano, J. Yang, S. Sun, "Development of a Novel Multi-Layer MRE Isolator for Suppression of Building Vibrations under Seismic Events", *Mechanical Systems and Signal Processing*, Vol. 70–71, pp 811–820, 2015.

54. Liu, Y., H. Matsuhisa, H. Utsuno, "Semi-Active Vibration Isolation System with Variable Stiffness and Damping Control", *Journal of Sound and Vibration*, Vol. 313, pp 16–28, 2008.

55. Sun, S., J. Yang, W. Li, H. Deng, H. Du, G. Alici, "Development of an MRE Adaptive Tuned Vibration Absorber with Self-Sensing Capability", *Smart Materials and Structures*, Vol. 24, 2015.

56. Ning, D., S. Sun, H. Du, W. Li, N. Zhang, "Vibration Control of an Energy Regenerative Seat Suspension with Variable External Resistance", *Mechanical Systems and Signal Processing*, Vol. 106, pp 94–113, 2018.

57. Sapiński, B., "Experimental Study of a Self-Powered and Sensing MR-Damper-Based Vibration Control System", *Smart Materials and Structures*, Vol. 20, pp 105007, 2011.

58. Lallart, M., É. Lefeuvre, C. Richard, D. Guyomar, "Self-Powered Circuit for Broadband, Multimodal Piezoelectric Vibration Control", *Sensors and Actuators A: Physical*, Vol. 143, pp 377–382, 2008.

59. Kela, L., P. Vähäoja, "Recent Studies of Adaptive Tuned Vibration Absorbers/Neutralizers", *Applied Mechanics Reviews*, Vol. 62, pp 060801, 2009.

60. du Plooy, N.F., P.S. Heyns, M.J. Brennan, "The Development of a Tunable Vibration Absorbing Isolator", *International Journal of Mechanical Sciences*, Vol. 47, pp 983–997, 2005.

61. Bueter, A., E. Janssen, S. Gaisbauer, "Device For the Purpose of Influencing the

Transfer of Vibration Between Two Units", US Patent no: 9644698, 2017.

62. Ivers, D.E., R.W. Wilson, "Self-Tuning Vibration Absorber System and Method of Absorbing Varying Frequency Vehicle Vibrations", US Patent no: 6983833, 2002.

63. Wallersteen, L., "Self Tuning Vibration Absorber", US Patent no: 2838137, 1958.

64. Sashida, T., T. Kenjo, *An Introduction to Ultrasonic Motors*, Clarendon Press, Oxford, 1993.

65. Ragulskis, K., R. Bansevicius, R. Barauskas, G. Kulvietis, *Vibromotors for Precision Microrobots*, Hemisphere Pub. Corp, New York, 1988.

66. Meirovitch, L., *Fundamentals of Vibrations*, McGraw-Hill, Boston, 2001.

67. Howell, L.L., S.P. Magleby, B.M. Olsen, *Handbook of Compliant Mechanisms*, John Wiley & Sons, Inc, Chichester, West Sussex ; Hoboken, 2013.

68. Su, H.-J., "A Pseudorigid-Body 3R Model for Determining Large Deflection of Cantilever Beams Subject to Tip Loads", *Journal of Mechanisms and Robotics*, Vol. 1, pp 021008, 2009.